

209056

JPRS-UEQ-87-009  
23 JUNE 1987



# ***JPRS Report***

# **Science & Technology**

***USSR: Engineering &  
Equipment***

19980701 146

**DISTRIBUTION STATEMENT A**  
Approved for public release;  
Distribution Unlimited

REPRODUCED BY  
U.S. DEPARTMENT OF COMMERCE  
NATIONAL TECHNICAL  
INFORMATION SERVICE  
SPRINGFIELD, VA 22161

DTIC QUALITY INSPECTED 1

33  
76  
AΦ5

23 JUNE 1987

Soviet books and journal articles displaying a copyright notice are reproduced and sold by NTIS with permission of the copyright agency of the Soviet Union. Permission for further reproduction must be obtained from copyright owner.

## SCIENCE & TECHNOLOGY

### USSR: ENGINEERING & EQUIPMENT

#### CONTENTS

##### SURFACE TRANSPORTATION

- Optimum Design of Some Structural Elements of Motor Vehicles  
From Fiber Polymer Composites  
(R.I. Nepershin, V.V. Klimenov; MASHINOVEDENIYE, No 6,  
Nov-Dec 86)..... 1

##### NUCLEAR ENERGY

- Optimization of Fuel Charge Layout in Water-Moderated Water-  
Cooled Power Reactor  
(V.D. Simonov, P.Ye. Filimonov; ATOMNAYA ENERGIYA, No 4,  
Oct 86)..... 10
- Experiment on Raising Burn-up Level in Fuel Assemblies of  
VVER-440 MW Water-Moderated Water-Cooled Power Reactor  
(Ye.I. Ignatenko, A.A. Matveyev, et al.; ATOMNAYA  
ENERGIYA, No 4, Oct 86)..... 11

##### INDUSTRIAL TECHNOLOGY

- Investigation of Stress Fields When Improving Assemblies of  
Grain Combines  
(N.A. Makhutov, N.I. Prigorovskiy, et al.;  
MASHINOVEDENIYE, No 6, Nov-Dec 86)..... 12
- Development and Investigation of Active Pneumatic Vibration  
Insulation Systems for Human Operator  
(A.V. Andreychikov; IZVESTIYA VYSSHIKH UCHEBNYKH  
ZAVEDENIY: MASHINOSTROYENIYE, No 2, Feb 87)..... 22

Application of Air Microjector in Vacuum Gripping Device of Industrial Robot (N.P. Zaporozhets; MEKHANIZATSIYA I AVTOMATIZATSIYA PROIZVODSTVA, No 12, Dec 86).....	28
Analysis of Possibility and Effectiveness of Using Composite Materials in Grain Combines To Reduce Weight (A.V. Berezin, V.G. Lyutsau, et al.; MASHINOVEDENIYE, No 6, Nov-Dec 86).....	31
New Machine Tool Products at NTP'86 (MEKHANIZATSIYA I AVTOMATIZATSIYA PROIZVODSTVA, No 9, Sep 86).....	37
Dynamics of Start-up of Arterial Heat Pipe From Frozen and Cooled-Down States (A.N. Abramenko, L.Ye. Kanonchik, et al.; INZHENERNO-FIZICHESKIY ZHURNAL, No 5, Nov 86).....	56
Dynamics of Ice Formation on Underground Pipelines (B.A. Krasovitskiy; INZHENERNO-FIZICHESKIY ZHURNAL, No 5, Nov 86).....	57

#### TURBINE AND ENGINEER DESIGN

Optimum Parameters of Pump-Turbine and Their Relation to Hydrodynamic Characteristics of Blade Rows (A.K. Malyshev, I.M. Pylev; ENERGO MASHINOSTROYENIYE, No 10, Oct 86).....	58
Estimating State of Stress for Design of Disks for Mixed-Flow Turbomachines (B.I. Berman, V.V. Litinetskiy; ENERGO MASHINOSTROYENIYE, No 10, Oct 86).....	59
Predicting Abrasive Wear of Centrifugal Smoke-Exhaust Fans and Grinding-Mill Blower (Yu.I. Abramov, B.A. Balusov; ENERGO MASHINOSTROYENIYE, No 10, Oct 86).....	59

#### HIGH-ENERGY DEVICES, OPTICS AND PHOTOGRAPHY

Defocusing of Mirror Systems During Uniform Temperature Variation (M.A. Gurbanyazov, I.I. Malysheva, et al.; IZVESTIYA AKADEMII NAUK TRUKMENSKOY SSR: SERIYA FIZIKO-TEKHNICHESKIKH, KHIMICHESKIKH I GEOLOGICHESKIKH NAUK, No 5, Sep-Oct 86).....	61
---	----

TESTING AND MATERIALS

Catalytic Activity of Nickel Coatings, Chemically Precipitated Onto Nonconducting Materials (L.N. Andreyeva, Zh.I. Bobanova; IZVESTIYA AKADEMII NAUK MOLDAVSKOY SSR: SERIYA FIZIKO-TEKHNICHESKIKH I MATEMATICHESKIKH NAUK, No 3, Sep-Dec 86).....	68
Briefs	
Cermet Glues	71
Metal Flaw Detection	71

/9835

OPTIMUM DESIGN OF SOME STRUCTURAL ELEMENTS OF MOTOR VEHICLES FROM FIBER POLYMER COMPOSITES

Moscow MASHINOVEDENIYE in Russian No 6, Nov-Dec 86 (manuscript received 30 Apr 86) pp 84-89

[Article by R. I. Nepershin and V. V. Klimenov, Moscow]

[Text] Replacement of metals with polymer composites, reinforced high-strength and high-modulus fibers results in a significant reduction of the weight of structural elements of transport vehicles and is one of the important trends of technical progress in modern machine building. Polymer composites are now used actively in manufacture of aircraft [1], for which a reduction of weight is of primary significance.

The high values of the specific strength and stiffness of polymer composites compared to structural metals stimulated a rapid increase of the volume of their production, which resulted in a significant reduction of the cost of these materials and in the possibility of using them in the automotive industry [2-4]. A reduction of the cost of the elements of composite structures and a reduction of the technological cycle of manufacturing them are important conditions for extensive use of composites in large-scale machine building. Economical use of these materials can be achieved by an efficient combination of composites, which have different mechanical characteristics and costs, in the design, depending on its functional designation. Optimum design of hybrid composite structure according to cost and weight criteria is of important practical significance.

The method and examples of optimal computer design of power composite elements of automotive structures (leaf springs and bumpers), which reduce to solution of the problem of nonlinear software engineering: find the optimal point  $\bar{x}^*$  in the space of variables of the design  $\bar{x}$ , at which the specific function  $f$ , which is a linear combination of weight  $f_1$  and cost  $f_2$

$$f(\bar{x}) = \alpha f_1(\bar{x}) + (1 - \alpha) f_2(\bar{x}), \quad 0 \leq \alpha \leq 1 \quad (1)$$

assumes the least value when the constraints on the following design variables are fulfilled

$$g_j(\bar{x}) \geq 0, \quad j=1, 2, \dots, m. \quad (2)$$

The accumulated experience of solving many optimum design problems showed that the sequential unconditional minimization method [5] using the expanded internal penalty function [6], which ensures stable operation of the minimum search algorithm near the boundary of the permissible area, is effective with a comparatively small number of design variables (up to 20) and with low labor intensiveness of computer calculation of the specific function and constraints (not more than 1 min). The search for the unconditional minimum is conducted by the method of Powell conjugate directions without calculating the derivatives in combination with the golden mean method [5, 7]. This considerably facilitates and accelerates the preparation and solution of practical and optimum design problems of composite structures with complex functional constraints in strength and stiffness. A combination of programs in FORTRAN, which permit one to solve different optimal design problems by connection of routines for calculation of specific function (1) and constraints (2), was worked out for computer solution of the nonlinear programming problem by sequential unconditional minimization with expanded internal penalty function.

The composite leaf spring. According to operating conditions of leaf springs, they are calculated for strength when a maximum transverse load  $P_{\max}$  is applied to the middle of the spring with regard to the dynamic overload factor and are calculated for stiffness, equal to the ratio of load to deflection in the middle of the spring. The spring loading diagram is shown in Figure 1, a. Calculations show that the required strength and stiffness can be achieved with considerably fewer number of plates when steel is replaced with polymer fiber composites during manufacture of leaf springs. Specifically, the additional leaf springs (spring cushions) of trucks can be two- or three-plate.

Multilayer plates of composites, having different properties (Figure 1, b), can be used to reduce cost. For example, the outside layers of glass fiber-reinforced plastic, having greater maximum deformations and strength in the direction of the fibers, intermediate layers of carbon fiber-reinforced plastic having greater stiffness and fatigue strength, and having a central layer, which should tolerate comparatively low tangential stresses due to transverse forces, can be fabricated from less expensive material. Thus, we produce a five-layer design of the plate.

Let us consider optimization of three-plate composite springs, consisting of five-layer plates with symmetrical arrangement of the layers with respect to the mid-plane (Figure 1). The length of the first plate  $2l_1$  and the width of the plates  $b$  are given by the design of the suspension. The lengths of the second  $2l_2$  and third  $2l_3$  plates can either be given or determined from calculation. Accordingly, the design variables in the problem under consideration are the thicknesses of the composite layers  $h_1$ ,  $h_2$  and  $h_3$  of each plate and the lengths of the second and third plates.

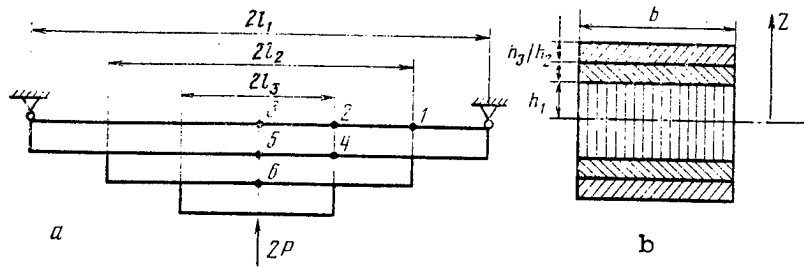


Figure 1

The functions of weight  $f_1$  and cost  $f_2$  in specific function (1) for a three-leaf spring have the form

$$f_1 = \frac{2b}{l_1} \sum_{i=1}^3 l_i \left( h_{1i} + \frac{\gamma_2}{\gamma_1} h_{2i} + \frac{\gamma_3}{\gamma_1} h_{3i} \right),$$

$$f_2 = \frac{2b}{l_1} \sum_{i=1}^3 l_i \left( h_{1i} + \frac{\gamma_2}{\gamma_1} \frac{\Pi_2}{\Pi_1} h_{2i} + \frac{\gamma_3}{\gamma_1} \frac{\Pi_3}{\Pi_1} h_{3i} \right),$$

where  $i = 1, 2, 3$  are the numbers of the plates,  $l_i$  are the half-lengths of the plates,  $h_{1i}$ ,  $h_{2i}$  and  $h_{3i}$  are the thickness of the composite layers of each plate,  $\gamma_1$ ,  $\gamma_2$  and  $\gamma_3$  are the specific weights of the materials comprising the composite plate and  $\Pi_1$ ,  $\Pi_2$  and  $\Pi_3$  are the costs of these materials.

The functional constraints on strength and stiffness are calculated according to rod theory on the basis of the hypothesis of plane cross sections, since the distance between supports far exceeds the thickness. The flexural stiffness of each plate is calculated from the condition of the compatibility of the deformations of layers

$$D_i = \frac{2}{3} b \sum_{k=1}^3 (Z_{ki}^3 - Z_{k-1,i}^3) E_{ki}, \quad i=1, 2, 3, \quad (3)$$

where  $i$  is the number of the plate,  $E_k$  is the modulus of elasticity of the material of layer  $k$  and  $Z_k$  are the coordinates through the thickness of the interfaces of the layers, calculated from the mid-plane.

A multileaf spring is calculated by the hypothesis of the equal curvature of the plates [8]. At given maximum force  $P_{\max} = 2P$  and stiffness of the plates  $D_i$ , we

calculate the greatest normal stresses  $\sigma_k$ ,  $k = 1, 2, 3$  in the composite layers of the first plate in the cross section, passing through the end of the second plate

$$\sigma_k = P(l_1 - l_2)Z_k E_k / D_1, \quad (4)$$

We calculate the stresses in the second and first plates in the cross section passing through the end of the third plate

$$\sigma_n = P(l_1 - l_3)Z_n E_n / (D_1 + D_2), \quad (5)$$

and we calculate the stresses in the first, second and third plates in the cross section passing through the middle of the spring

$$\sigma_h = Pl_1 Z_h E_h / (D_1 + D_2 + D_3). \quad (6)$$

The points at which the strength along the normal stresses is checked are shown in Figure 1, a. We add the temperature stresses, related to the difference of the thermal expansion coefficients of the composite layers, to the normal stresses, calculated by formulas (3)-(6). We calculate the greatest tangential stress  $\tau$  by the Zhuravskiy formula in the mid-point through the thickness of the first plate. We find 19 strength restrictions at the given values of the permissible normal stresses  $[\sigma]_k$  of the composite layers and the permissible tangential stress  $[\tau]$ . The stiffness of a three-leaf spring is equal to

$$C = 3 \left[ \frac{(l_1 - l_2)^3}{D_1} + \frac{(l_1 - l_3)^3 - (l_1 - l_2)^3}{D_1 + D_2} + \frac{l_1^3 - (l_1 - l_3)^3}{D_1 + D_2 + D_3} \right]^{-1}. \quad (7)$$

We find the last functional constraint--equality--at given value of stiffness  $[C]$ , which should be equal to the calculated value of (7). Moreover, there should be design-technological constraints on the permissible thickness of the composite layers and on the lengths of the second and third plates. As a result, we find 32 constraints and 12 design variables in the optimum design problem of a three-leaf composite spring.

The optimal design problem of composite leaf springs is realized in the form of a FORTRAN program. Machine time expenditures on the BESM-6 computer for four steps of sequential unconditional minimization with minimum search accuracy of 0.01 comprise approximately 80 seconds. The spring cushions of GAZ-53, MAZ-500 and ZIL-130 trucks are optimized by the developed program in the case of their

being manufactured from carbon fiber-reinforced plastics: central layer and outer layers of glass fiber-reinforced plastic in each plate and intermediate layers of carbon fiber-reinforced plastic. The properties of composites and their costs are taken from [2, 9]. The permissible normal stresses are assumed equal to 600 MPa for glass fiber-reinforced plastic and 800 MPa for carbon fiber-reinforced plastic. Calculation showed that the prevalent thickness of lighter carbon fiber-reinforced plastic is found upon optimization by weight ( $\alpha = 1$  in the specific function (1)), but the stiffness and cost of the spring are extremely high. The optimum design at  $\alpha < 1$  is slightly dependent upon  $\alpha$ , the thickness of carbon fiber-reinforced plastic is equal to the minimum value  $[h] = 1.5$  mm and the stiffness of the spring is equal to the given value with accuracy of 1-3 percent. The outer fibers of the external glass fiber-reinforced plastic layers are loaded to the maximum normal stress, the carbon fiber-reinforced plastic layers are also rather highly loaded, while the central glass fiber-reinforced plastic layer is weakly loaded both by normal and by tangential stresses. The optimum thickness of composite layers  $h_1, h_2$  and  $h_3$ , the thickness of the plates  $H = 2(h_1 + h_2 + h_3)$  and the weight of three-layer carbon-glass fiber-reinforced plastic spring cushions of GAZ-53 trucks ( $P_{\max} = 25.4$  kN,  $[C] = 1.9$  kN/cm,  $b = 65$  mm), MAZ-500 trucks ( $P_{\max} = 29.4$  kN,  $[C] = 1.97$  kN/cm,  $b = 90$  mm) and ZIL-130 trucks ( $P_{\max} = 36.6$  kN,  $[C] = 1.83$  kN/cm,  $b = 75$  mm) for  $\alpha = 0.5$  are presented in the table. Composite spring cushions are four-sixfold lighter than steel spring cushions.

Марка (1) автомобиля	Помер(2) листа	Длина листа, мм (3)	$2h_1$ , мм	$h_2$ , мм	$h_3$ , мм	$H$ , мм	(4) Вес, Н
(5) ГАЗ-53	1	1050	4.5	1.5	7.5	22.5	} 50
	2	700	4.3	1.5	2.1	11.5	
	3	400	6.2	1.5	7.4	24.0	
(6) МАЗ-500	1	1000	4.3	1.5	6.1	19.5	} 58
	2	700	4.3	1.5	2.3	12.0	
	3	400	4.4	1.5	5.7	18.8	
(7) ЗИЛ-130	1	1050	4.4	1.5	7.4	22.2	} 54
	2	700	4.3	1.5	2.1	11.6	
	3	400	4.5	1.5	6.4	20.2	

Key:

- |                        |            |
|------------------------|------------|
| 1. Make of truck       | 5. GAZ-53  |
| 2. Number of plate     | 6. MAZ-500 |
| 3. Length of plate, mm | 7. ZIL-130 |
| 4. Weight, N           |            |

The composite bumper. The functional designation of the bumper of a compact automobile is absorption of its kinetic energy without residual strains and damage in the case of collision with an obstacle when the automobile is moving at given initial speed, specified by international standards. Let us simulate the bumper by a long beam of trough-shaped cross section with flexible supports, which simulate the stiffness of the body (Figure 2). The design variables are

dimensions  $h$ ,  $b$  and  $\delta$  of the cross-sectional profile of the beam (Figure 2, c). Depending on the design of the bumper, the load tolerated by it upon collision with an obstacle can be transmitted either in the form of two concentrated forces  $P/2$  or in the form of a distributed load  $q$  on length  $l$  (Figure 2, a and b). These loads are calculated from the equality of the kinetic energy of the moving automobile of the potential energy of the flexible bumper-body system

$$P = v [2M / (A_1 / 24EJ_x + 1/C_1)]^{1/2}, \quad A_1 = (L-l)^2(L+2l),$$

$$q = v [2M / (A_2 / 24EJ_x + 1/C_1)]^{1/2}, \quad A_2 = l^2 \{L^3 - l[2l^2 - 0.35l(5L-l)]\},$$

where  $v$  is the speed of the automobile when it meets the obstacle,  $M$  is the mass of the automobile,  $E$  is the modulus of elasticity of the bumper material,  $L$  is the distance between supports,

$$J_x = \delta \left\{ (h+\delta) \left( y_0^2 + \frac{b^2}{4} \right) + \frac{2}{3} \left[ \left( y_0 - \frac{\delta}{2} \right)^3 - (y_0 - b)^3 \right] \right\}$$

is the moment of inertia of the cross section and  $y_0 = (b^2 - \delta^2/4)/(h + 2b)$ .

We did find the maximum flexure  $w$ , the greatest normal stresses  $\sigma$  and tangential stresses  $\tau$  in the transverse section for the following concentrated forces from the theory of bending of thick rods [11]

$$w = \frac{P(L-l)}{96EJ_x} [2L(L+l) - l^2], \quad \sigma = \frac{P}{4J_x} (L-l)(b-y_0), \quad \tau = \frac{P}{4J_x} (b-y_0)^2$$

and for distributed load

$$w = \frac{ql}{192EJ_x} [L(2L^2 - 3Ll + 4l^2) - l^3], \quad \sigma = \frac{ql^2}{4J_x} (b-y_0),$$

$$\tau = \frac{ql}{4J_x} (b-y_0)^2.$$

The specific function in the constraints of the nonlinear programming problem (1) and (2) have the form  $f = 2b + h - \gamma\delta$ ,  $g_1 = [w] - w$ ,  $g_2 = [\sigma] - \sigma$ ,  $g_3 = [\tau] - \tau$ ,  $g_4 = h - [h]$ ,  $g_5 = [b] - b$  and  $g_6 = \delta - [\delta]$ , where the brackets denote the permissible values, when a bumper is manufactured from homogeneous material.

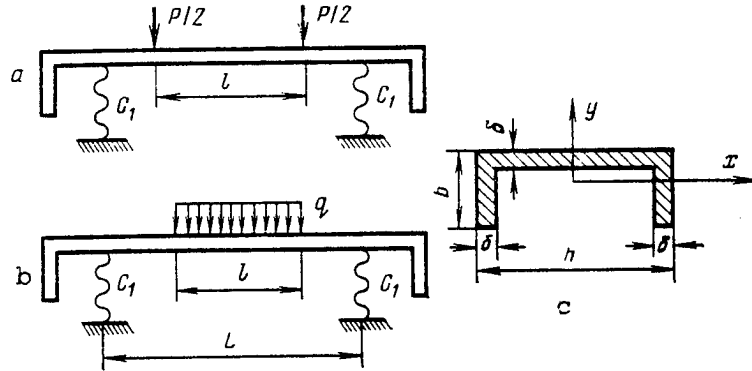


Figure 2

The method of optimum design of a bumper in the described postulation is realized in the form of a FORTRAN program. Machine time expenditures on the BESM-6 computer for four steps of sequential unconditional minimization with minimum search accuracy of 0.01 comprises approximately 5 seconds.

The bumper of a compact automobile of medium class, manufactured from glass fiber-reinforced plastic and structural steel, is optimized to estimate the weight efficiency when using polymer composites. The weight of the automobile is equal to 16 kN, the speed upon encountering an obstacle is 4 km/hr, the length of the bumper is 1,400 mm,  $[w] = 30$  mm  $[b] = 125$  mm,  $[h] = 150$  mm and  $[\delta] = 3$  mm. The calculations were made for concentrated load in the center of the bumper and for distributed load on length of  $l = 70$  mm. The flexible strength characteristics and specific weight are taken as  $E = 40$  GPa,  $[\tau] = 40$  MPa,  $[\sigma] = 500$  MPa and  $\gamma = 0.2 \cdot 10^{-1}$  N/cm<sup>3</sup> from [9] for glass fiber-reinforced plastic and  $E = 210$  GPa,  $[\tau] = 250$  MPa,  $[\sigma] = 500$  MPa and  $\gamma = 0.78 \cdot 10^{-1}$  N/cm<sup>3</sup> from [11] for structural steel. The optimum dimensions and weight per unit length of the bumper were found as a result of the calculations. The distributed load is  $b = 123$  mm,  $h = 150$  mm,  $\delta = 6.1$  mm and  $G = 1.9$  N/cm for steel and  $b = 66$  mm,  $h = 150$  mm,  $\delta = 7.3$  mm and  $G = 0.41$  N/cm for glass fiber-reinforced plastic; the concentrated load is  $b = 124$  mm,  $h = 150$  mm,  $\delta = 3.7$  mm and  $G = 1.17$  N/cm for steel and  $b = 124$  mm,  $h = 150$  mm,  $\delta = 3.1$  mm and  $G = 0.24$  N/cm for glass fiber-reinforced plastic.

The active constraint in optimization of a steel bumper is strength according to normal stress. When a glass fiber-reinforced plastic bumper is optimized as a function of the type of load, the active elements are constraints on stiffness and on the permissible normal and tangential stresses. Upon concentrated application of load, the energy-absorbing capacity of the bumper is higher than with distributed application of load on a length of  $l = 70$  mm, which permits a considerable reduction of weight of the bumper, the dimensions of which are determined mainly by the strength along normal stresses. The use of glass fiber-reinforced plastic instead of structural steel at equal values of the permissible normal stress reduces the weight of the bumper by a factor of 4.8.

Conclusions. Effective high-speed programs for optimal computer design of composite structures of leaf springs and bumper of an automobile according to cost and weight criteria were developed with regard to different functional and structural-technological constraints that occur in practice.

The main characteristics of composite materials that affect the optimum designs of the considered structural elements are the moduli of elasticity, the permissible stresses along the normal and tangential stresses, specific weight and specific cost.

The examples of optimum design of composite leaf springs and bumper show the possibility of reducing their weight by a factor of 4-6 compared to steel structures.

#### BIBLIOGRAPHY

1. Rabotnov, Yu. N., A. A. Tupolev, V. F. Kutinov et al., "Using Carbon Fiber-Reinforced Plastics in Aircraft Designs," MEKHANIKA KOMPOZITNYKH MATERIALOV, No 4, 1981.
2. Kats, G. S., and D. V. Milevski, "Napolniteli dlya polimernykh kompozitnykh materialov" [Fillers for Polymer Composite Materials], Moscow, Izdatelstvo "Khimiya", 1981.
3. Chase, V. A., "Automotive Applications of Composite Materials," 11-th National SAMPE Technical Conference, Boston, Massachusetts, November 13-15, Vol, 1979.
4. Rugg, C., "Carbon and Aramid Reinforced Plastics in the Manufacture of Automotive Propeller Shafts," CIBA-GEIGY, Basel, 1982.
5. Fiacco, A., and G. MacCormick, "Nelineynoye programmirovaniye. Metody posledovatelnoy bezuslovnoy minimizatsii" [Nonlinear Programming. Methods of Sequential Unconditional Minimization], Moscow, Izdatelstvo "Mir", 1972.
6. Cassis, J. H., and L. A. Schmit, "On Implementation of the Extended Interior Penalty Function," INTERNATIONAL JOURNAL FOR NUMERICAL METHODS, Vol 10, 1976.
7. Moiseyev, N. N., Yu. P. Ivanilov and Ye. M. Stolyarova, "Metody optimizatsii" [Optimization Methods], Moscow, Izdatelstvo "Nauka", 1978.
8. Parkhilovskiy, N. G., "Avtomobilnyye listovyye resory" [Automotive Leaf Springs], Moscow, Izdatelstvo "Mashinostroyeniye", 1972.
9. "Composite Materials," "Analiz i proyektirovaniye konstruktsiy" [Analysis and Design of Structures], Vol 7, Part 1, Moscow, Izdatelstvo "Mashinostroyeniye", 1978.

10. Rabotnov, Yu. N., "Mekhanika deformiruyemogo tverdogo tela" [The Mechanics of a Deformable Solid], Moscow, Izdatelstvo "Nauka", 1979.
11. "Spravochnik po mashinostroitel'nykh materialam. Tom 1. Stal" [Handbook on Machine-Building Materials. Volume 1. Steel], Moscow, Mashgiz, 1959.

COPYRIGHT: Izdatelstvo "Nauka", "Mashinovedeniye", 1986

6521

CSO: 1861/102

OPTIMIZATION OF FUEL CHARGE LAYOUT IN WATER-MODERATED WATER-COOLED POWER REACTOR

Moscow ATOMNAYA ENERGIYA in Russian Vol 61, No 4, Oct 86  
(manuscript received 16 Sep 85, in final version 16 Jan 86) pp 237-240

[Article by V.D. Simonov and P.Ye. Filimonov]

[Abstract] The problem of optimizing the fuel assembly layout in the reactor core is treated as a mathematical problem of optimization with respect to a minimizable target functional, this functional being either nonuniformity of the power distribution among discrete fuel elements or leakage of neutrons through the lateral surface of the reactor core. Formulation and solution of this problem are particularized for VVER (water-moderated water-cooled thermal) reactors. The procedure involves analytical description of the properties of the target functional and selection, on this basis, of the optimum layout from the discrete set of layouts under consideration. Calculations are based on the one-group steady-state reactor equation containing a neutron multiplication coefficient, which factors in the influence of boron and energy release distribution. Assuming constant neutron flux, the distribution of properties is described by an "etalon" function corresponding to a unique invariant in the space of multiplying properties (the set of critical states). Calculations by the BIPR-5 program designed for three-dimensional energy release and fuel depletion fields in the one-group diffusion approximation have been made for water-moderated water-cooled power reactors. Figures 2; references 3: all Russian.

2415/9835  
CSO: 1861/99

EXPERIMENT ON RAISING BURN-UP LEVEL IN FUEL ASSEMBLIES OF VVER-440 MW .  
WATER-MODERATED WATER-COOLED POWER REACTOR

Moscow ATOMNAYA ENERGIYA in Russian Vol 61, No 4, Oct 86  
(manuscript received 31 Oct 85) pp 240-242

[Article by Ye.I. Ignatenko, A.A. Matveyev, Yu.N. Pytkin, M.V. Panin,  
V.A. Voznesenskiy, and V.N. Proselkov]

[Abstract] An experiment was performed at the Kola AES on intensifying the utilization of nuclear fuel in VVER-440 MW water-moderated water-cooled power reactors, this being achievable with more frequent partial overloading and concurrently longer total fuel burning periods. The experiment was run in three stages, on the basis of preliminary analysis and theoretical calculations. The first stage provided data on maximizing the enrichment of  $^{235}\text{U}$  adequately for four, rather than the customary three, overloading cycles. The second stage provided data on the stability of fuel assemblies during the added fourth overloading cycle. In the third and last stage the number of makeup fuel elements was reduced, on the basis of favorable results in the preceding stage, and the reactor remained operative through all four overloading cycles. An average 36.2 kg/t burn-up level in steady operation was reached with maximally 3.6%-enriched  $^{235}\text{U}$ . Operation in the industrial mode was continued with four overloading cycles annually and a 4-year fuel burning period was gradually attained by planning up to nine fuel "cycles" between replacements of elements. Figures 1; tables 2; references 1: Russian.

2415/9835  
CSO: 1861/99

INVESTIGATION OF STRESS FIELDS WHEN IMPROVING ASSEMBLIES OF GRAIN COMBINES

Moscow MASHINOVEDENIYE in Russian No 6, Nov-Dec 86 (manuscript received 27 Jun 86) pp 76-83

[Article by N. A. Makhutov, N. I. Prigorovskiy, A. N. Salin and Yu. V. Shumakov, Moscow]

[Text] Increasing the service life of grain combines and of other agricultural machinery and reducing their metal consumption requires the corresponding scientific research and experimental work. Upon improvement of supporting structures, one must determine the real or near-real values of strains and stresses in the components of these structures, which occur during their operation. The complexity of the structures and their stress-strain states render solution of problems only by calculation inadequate, but require the use of experimental methods with subsequent measurements during bench and operating tasks of full-scale structures and tests on models. A wide range of investigations is conducted with regard to the increase of requirements on the operating parameters of agriculture machines and for optimization of their load-bearing structures to establish the calculated load conditions and to study the stress-strain states and vibrations and to estimate strength during static and dynamic loads. The cycle of these investigations at the design stage and at the stage of improving the structural assemblies of agriculture machines includes experimental study (on benches and models) of the load strains and stresses, established from data of operational tests, obtained by tensometry and dynamometry..

Modern experimental methods of strain and stress investigation permit one to determine the real values of strains, displacements and forces in machine and structural parts. There are a considerable number of experimental methods, distinguished by the physical principle on which they are based, and by their own capabilities with regard to the variety of problems, conditions and types of stress states. Some of the effective methods among those of determining the strain and stress fields in parts and structures of agricultural machines, including grain combines, are the method of brittle strain-sensitive coatings and the polarization-optical method [1].

The method of brittle stain-sensitive coatings is the more operative in these problems during bench and full-scale tests, especially when studying the stress-

strain states of the surfaces of complex three-dimensional structures of agricultural machines, and is used both in the design stage of structures and in the stage of modification and improvement according to strength conditions. It permits one to find the main stresses with error in the range of  $\pm 15$  percent, without resorting to other measurement methods, in loaded zones, including stress concentration points, with the possibility of a smooth increase of the load of the structure under investigation or the use of brittle coatings of different strain sensitivity. The coatings are used when investigating parts and structures of any shape, of any material and of models of them with relative elongations at measurement points in the range from  $1 \cdot 10^{-4}$  to  $1 \cdot 10^{-2}$ . It is easy to find low-load zones, the directions of the main strains in the loaded zones and the values of the stress concentration factors on the surface of the zone of highest strains, compared to other methods. The small thickness of the coating (0.1 mm) permits one to measure the strains during larger gradients on the surface. The fields of elastoplastic strains can also be measured and the stresses can be estimated by using the strain pattern of the part material.

Types of brittle strain-sensitive coatings, developed at the Institute of Machine Science, USSR Academy of Sciences [2], cover a wide range of temperatures during testing: 1)  $5-40^\circ$  (colophony-type coating, hot spraying); 2)  $-196$  to  $200^\circ$  (oxide coatings, glued); 3)  $100-400^\circ$  (enamel, baked on the part).

Colophony-type coatings, applied by flame spraying and which are very efficacious in conducting such experiments, have limitations under test conditions--climatic temperatures from  $5$  to  $40^\circ$  and low temperature ( $\pm 3^\circ$ ) and humidity fluctuations; a crack in the coating with excess ratios of the main stresses at the measurement point occurs at a specific value of main tensile stress, determined by calibration. Glued oxide coatings for measurements at temperature in the range from  $-196$  to  $+200^\circ$  are used upon temperature fluctuations within the indicated range and in the presence of water and oils; a crack at the point of the coatings occurs at a specific value of main strain, determined by calibration. An enamel coating, baked on the part, is thermo-compensated for measurements of titanium alloys upon measurements at  $100$  to  $400^\circ\text{C}$ .

The polarization-optical method of investigation of stresses, used widely, permits one to find the strain and stress fields through flat and three-dimensional models, made similar in shape and at loading of the part or structure to be investigated and illuminated by polarized light. The advantages of the method are the possibility of obtaining the stress and strain fields through the cross sections and inside the model, of making measurements in the concentration zones of very small bases, high accuracy, good clearness of the method and simplicity of the measurements. When solving engineering problems when one must find the stresses on an unloaded surface of a three-dimensional and flat elastic model, observations in polarized light are sufficient. The stresses in a full-scale structure can easily be calculated by similarity formulas for measured stresses in the elastic model. The main advances of the past few years in development of the method include working out solutions of the three-dimensional elastic problems and practical application of them (methods of

recording strains, composite models, scattered light method, integrated photoelasticity), joint use of the polarization-optical method with other experimental methods and numerical calculation on the computer, including separate determination of the main stresses, methods of investigation of stresses during pulsed loads and thermoelastic stresses, methods of investigation of strains and stresses in nonlinear problems of elasticity, plasticity and creep on the model materials and investigation of stresses using the invisible part of the spectrum.

The stresses in the universal joint of the reaper and in the casings of the drive wheel axles of grain combines were investigated using brittle strain-sensitive coatings.

Universal joint of the combine reaper. To investigate the universal joint of the reaper, a brittle colophony coating was applied to the entire external surface of the universal joint with the exception of the contact zones. The universal joint was loaded for one of the structures by stepped application of torque  $M$  from 0 to 600 N·m every 50 N·m (strain kept within elastic limit). The coating was repeatedly calibrated during the tests and its strain sensitivity  $\sigma_0 = 140$  MPa (with variation in the range of  $\pm 15$  percent) was determined. The first cracks in the brittle coating were recorded at  $M_1 = 350$  N·m on the forks of the universal joint within the zones shown in Figure 1 by the dashed curve (isoentat 1). The boundaries of crack propagation on the surface of the forks at greater torque  $M_2 = 400$  and  $M_3 = 600$  N·m and the isoentats 2 and 3, corresponding to these loads (Figure 1), were noted in similar fashion. The first cracks also appeared on the smooth part of the rod with square cross section at maximum load of  $M_3 = 600$  N·m. Cracks did not appear in the brittle coating on the tubular part of the universal joint at maximum torque. Thus, the greatest tensile stresses in the loaded zones of the universal joint, where cracks occur in the brittle coating, were determined from the data. Thus, the maximum tensile stresses  $\sigma_1$  at torque of  $M_3 = 600$  N·m are determined on isoentats 1, 2 and 3 by proportional calculation from the functions:  $\sigma^{(1)}_1 = \sigma_0 M_3/M_1 = 240$  MPa and similarly  $\sigma^{(2)}_1 = 210$  and  $\sigma^{(3)}_1 = 140$  MPa. The stress-strain diagram of the maximum tensile stresses on the surface of the fork of the universal joint through cross section 0-0 at  $M = 600$  N·m is presented in Figure 1. The stresses in the universal joint were thus determined and it was established that the stresses are twofold greater in the most loaded zones of the fork of the universal joint than in the rod part of the universal joint. The unequal strength of the structure is shown and it was improved.

Axle casing of the combine. The stresses in the axle casing of the drive wheels of a grain combine were investigated by using brittle coatings during bench tests. Three versions of the axle casing of a stamped-welded design of different configurations and metal consumption were investigated to compare them according to the stress-strain state and to select the optimum design version for subsequent modification and optimization according to strength conditions. The characteristic features of these investigations were that the axle casings had large overall dimensions (the total surface area of each axle, where the stresses had to be measured, was approximately 3 m<sup>2</sup>) and complex shape (radius transitions, prejoined brackets and so on), which would require significant time

and money expenditures for measurements when using other experimental methods of stress determination. The measurements were made under conditions similar to a "sea climate" (temperature of 25°, humidity greater than 90 percent).

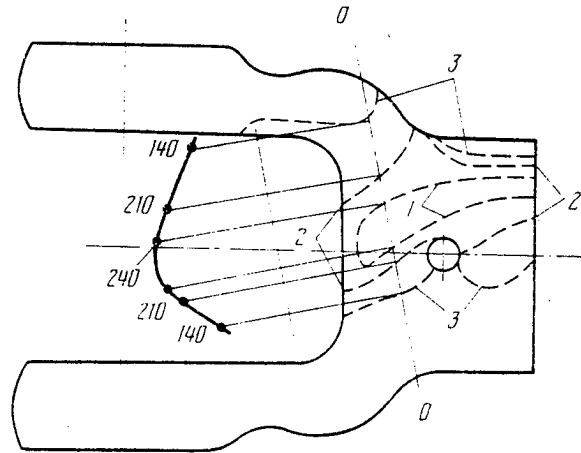


Figure 1

To determine stresses in compression zones, the brittle coating was applied to the axle, pre-stressed to the maximum values by force  $Q$  and by twisting moment  $M_{kp}$ , after which the axle was relieved in steps. The zones of the appearance and propagation of cracks and their directions were recorded for each stress (relief) step and the most typical crack patterns in the brittle coatings were photographed. The stresses were distributed with quantitative estimation over the entire outside of the versions of the casing as a result of investigating them by using brittle coatings. It was established that very irregular stress distribution with high gradient and level of stresses in the radius transition zones and in the brackets where the units are attached occurred in casing structures with symmetrically expanding mid-part. A new casing design was worked out from the results and from the recommendations. The level of maximum stresses in the concentration zones did not exceed 260 MPa in this version, used to work out a standardized axle for grain combines, with a 1.5-fold increase of the maximum loads on the casing. The weight of the casing, compared to the previous versions, was increased by no more than 15 percent.

The standardized axle. Development of a standardized axle of drive wheels is envisioned in development of new highly efficient grain combines as one of the most important and crucial assemblies of these machines. The problem of developing a standardized axle includes the need to ensure strength and the given surface life with regard to a wide range of possible operating loads. A combination of calculated and experimental estimates during design were made to solve this problem.

Optimization of the load-bearing part of the standardized axle was achieved by sequential use of methods of brittle strain-sensitive coatings and strain

measurements. Brittle strain-sensitive coatings were used to determine the greatest main stresses  $\sigma_1$  in local zones of their concentration by observing cracks in the coating. The greatest stresses at individual points were refined by strain measurements. The experimental investigations were performed on a special bench, which simulates the real operating load of the load-bearing part--the beam of the standardized axle. The power hydraulic cylinders were given a stepped increase (decrease) of load, creating axles that bend in two planes and twisting moments on the housing, not exceeding the maximum values in operation.

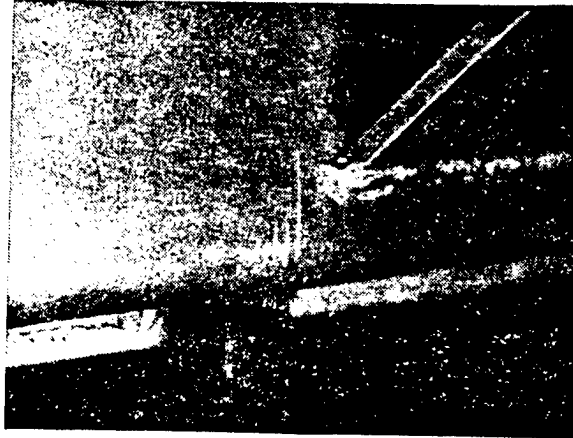


Figure 2

In the experiments, the brittle strain-sensitive coatings were applied immediately in all the zones of the axle casing to be investigated. After the coating was applied, the load was increased in steps with visual observation of the first occurrences of cracks in the zones and recording the ends of the cracks in the coating (isoentats), corresponding to the same values of  $\sigma_1 = \sigma_0$ , directed along the normal to the cracks, at each value of load. The first cracks formed in the zone of the beginning of seams of the bottom cover plates of axle box attachment and of the hydraulic cylinders for lifting the reaper part (Figure 2) at load of  $P = 50$  kN on the power hydraulic cylinder. An increase of the applied load is accompanied by an increase of the length of these cracks and by formation of other cracks near these cracks. A further increase of load to maximum operating loads of  $P = 98$  kN results in formation of a pattern of stress fields. The highest normal stresses for all the zones are presented in Figure 3.

Analysis of the results of investigations of stress fields made it possible to establish that the greatest stresses occur at the points of attachment of the transmission shift box to the axle beam, of the support brackets of the reaper part, in the zones of variation of the beam cross section in the axles of the beginning or end of a weld seam and of attachment of cover plates on the elongated bottom fibers (zones I-IV, Figure 3). The stresses at these points may reach 170 MPa at maximum operating loads.

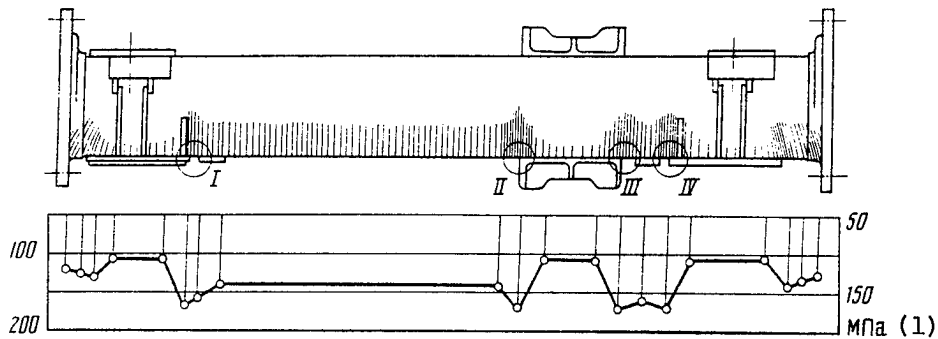


Figure 3

Key:

1. MPa

Analysis of the data obtained by using brittle coatings and the results of calculations showed that accumulation of damage over a 10-year operating life of the axle of the structure under consideration will not exceed the permissible value. A further increase of the life or a reduction of metal consumption is possible if the effect of stress concentrators in the weld seams on the bottom flange of the beam is reduced and if there is a sharp variation of the beam cross section.

Drive wheel and shaft axles of the rocker plate mechanism (MKSh) of the grain combine reaper. Investigation of the stress-strain states in these assemblies of combines is most feasible when using the polarization-optical method on three-dimensional models. This method can be used with regard to the complexity of the shape of the part to be investigated, which results in significant irregularity of stress distribution and of stress concentration and also in the presence of other integrated elements. The "freezing" method in combination with the scattered light method were used when investigating the stresses in the drive wheel axle of the combine [1]. To do this, two models of the drive wheel axle were developed (Figure 4) with bending and torsional load, respectively. The scale of geometric similarity for the models was selected as 1.33, i.e., the models were made in a form, reduced somewhat compared to the full-scale model. The shape of the drive wheel axle in the model was precisely reproduced. The models were fabricated from annealed blocks of ED-20M material by machining on metalcutting tools using a highly sharpened tool. The stresses were investigated upon action of loads of  $P = 18,000 \text{ N}$  and  $F = 103,000 \text{ N}$  and of the corresponding torque of  $M_x = 11,000 \text{ N}\cdot\text{m}$  on the axle of a full-scale structure. The parts integrated with the axle are received freely inserted and having a gap between them. The carrier was integrated with the axle, as in a full-scale structure, through a splined joint when fabricating the model.

Loading units, all elements of which, like the model, are fabricated from ED-20M epoxide material, were used to load the model of the axle during "freezing."

This eliminates distortion of the strain field, "frozen" in the model, due to the difference of the linear expansion coefficients of the model and elements of the loading units during heating of them when they are "frozen." The three-dimensional model with "frozen" deformations was cut into sections to determine the stresses. The arrangement of the sections in the model was selected so as to obtain the necessary information with minimum number of cuts. The considered models are bodies of rotation and have a plane of symmetry both in shape and with respect to the applied loads. Therefore, sections were cut from the model through the planes of symmetry.

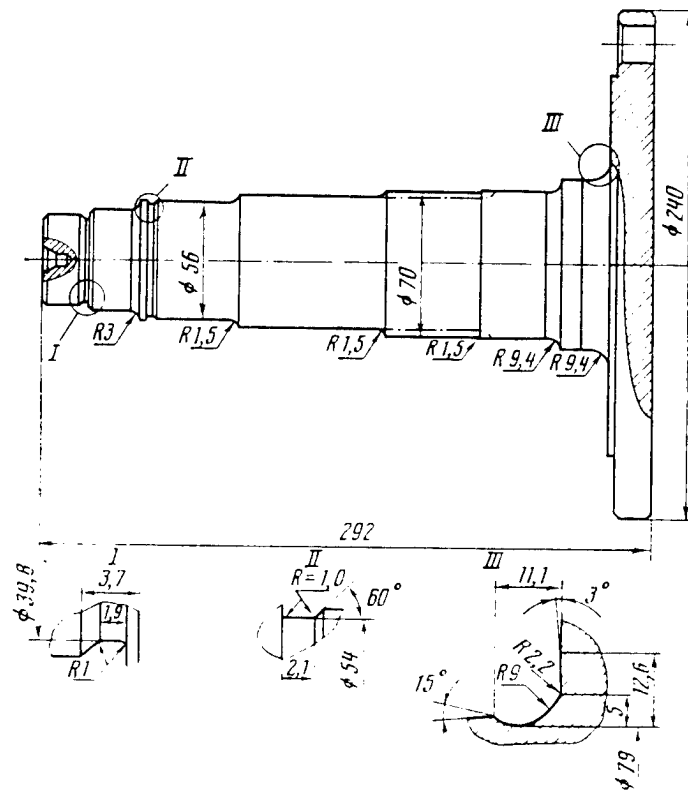


Figure 4

Stresses in the model, which were recalculated to a full-scale structure by the formula  $\sigma_H = \sigma_M \beta / \alpha^2$ , were found from measurements on the cutoff. Here  $\sigma_H$  and  $\sigma_M$  are the stresses in the full-scale structure in the model, respectively, and  $\alpha = l_H / l_M$  and  $\beta = P_H / P_M$  are the scales of the geometric and power similarity.

The stresses, found from the effect of bending and torsional moments in a full-scale axle of one of the combine structures, are represented in the form of stress-strain diagrams in Figure 5 ( $F = 103,000 \text{ N}$ ,  $P = 18,000 \text{ N}$ ) and in Figure 6 ( $M_{kp} = 11,000 \text{ N}\cdot\text{m}$ ). The small circles on these stress-strain diagrams note the

stresses in the axle, found by calculation from formulas of the resistance of materials.

Thus, the investigations made it possible to establish the distribution and value of stresses in the axle of the drive wheel of a grain combine during the effect of loads used in the calculation. The values of the stress concentration factors, which have a value of  $K = 1.3$  (tension) and  $K = 1.5$  (compression) in the most stressed section, were established. The greatest tensile stress during bending in the axle (Figure 5) does not exceed  $\sigma = 160$  MPa with regard to stress concentration. These stresses operate in the fillet, along which the smooth part of the shaft (81.5 mm in diameter, Figure 4) mates with the part of the shaft having an involute spline. The greatest tangential stresses upon loading of the axle by a twisting moment act in the fillet adjacent to the flange on the edge of the wheel axle and reach  $\tau = 85$  MPa.

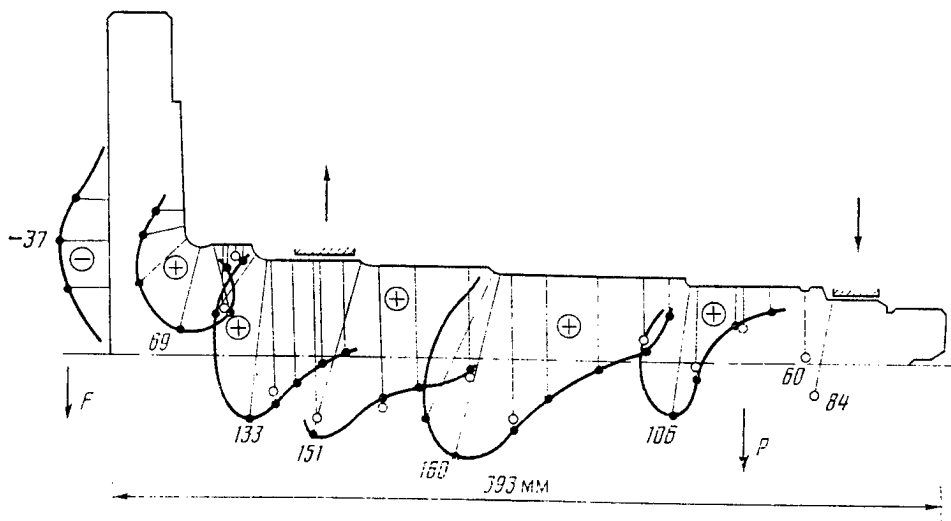


Figure 5. Stress Diagram  $\sigma$  (MPa) in Axle of Drive Wheel Due to Bending

The results of stress investigation permit one to refine the strength calculation of the axle structure and have the following capabilities of reducing the metal consumption of the axle structure in the lesser stressed zones: a decrease of axle diameter, decrease of the thickness of the flange wall and use of a welded axle structure (joining the flange wall to the axle). The corresponding design modification of these proposals is required.

The stress state in the stress concentration zone in the shaft of the rocker plate mechanism was investigated for two versions of the coupling zone near the bearing support (Figure 7;  $M = 1,089$ ,  $M' = 1,089$  N·m and  $F = 1,044$  N) by using the "freezing" method. It is shown that the first version of the coupling (a) yields the worst results due to the greater stresses. Variation of the shape of the transition zone of the shaft (b) results in a decrease of concentration of meridional stresses in the considered zone by a factor of 2.

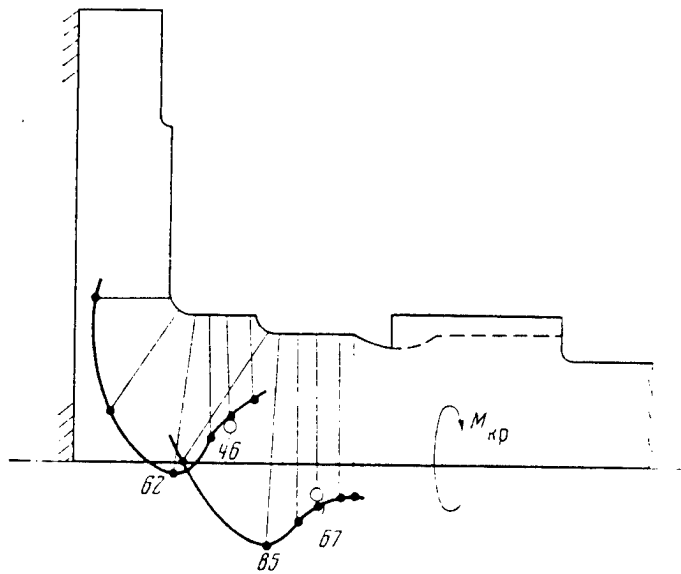


Figure 6. Tangential Stress Diagram in Axle of Drive Wheel Due to Torsion  $\tau$  (MPa)

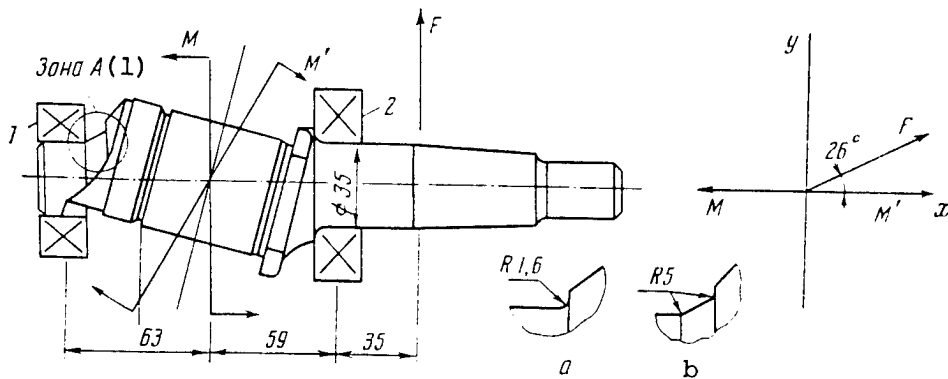


Figure 7

Key:

1. Zone

Meridional stress diagrams in the plane of symmetry of a full-scale part of the shaft of the rocker plate mechanism upon loading of it by bending moment  $M = 1,089 \text{ N}\cdot\text{m}$  are presented in Figure 8 for the second considered version of the shaft of the rocker plate mechanism. The greatest stresses in the coupling zone of the shaft elements, performed according to the second version, having a value of  $\sigma_m = 72 \text{ MPa}$  in the full-scale part near the bearing support. The annular stresses in the investigated models are maximum in the same zones as the meridional stresses and comprise 30-40 percent of the meridional stresses in these zones.

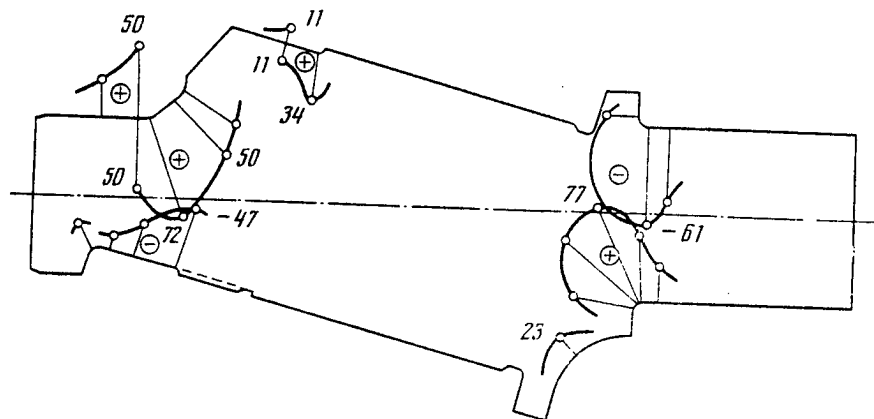


Figure 8

Besides the considered zone, one must take into account the zone of the fillets upon transition to a fit diameter of 35 mm near the bearing seat. The meridional stresses, found for this zone in the model, have approximately the same value as in the zone of the radial bearing. However, taking into account that a torsional moment acts on the shaft of the rocker plate mechanism near the bearing seat upon transition to fit diameter of 35 mm, besides a bending moment, one should regard this zone as the determining zone for the strength of the part.

The investigations conducted on flat models show that variation of the radii of this zone from 6 to 3 mm (these radii are equal to 5 mm in the full-scale part) does not result in an increase of stresses in the zone under consideration with a shape of a contour of a plane model, which corresponds to the contour of a part with transition zone, made according to version b (Figure 7).

The investigations permit one to conclude that the shape of the transition zone in the considered design was selected correctly.

#### BIBLIOGRAPHY

1. Prigorovskiy, N. I., "Metody i sredstva opredeleniya poley deformatsiy i napryazheniy" [Methods and Means of Determining the Strain and Stress Fields], Moscow, Izdatelstvo "Mashinostroyeniye", 1983.
2. Prigorovskiy, N. I. and V. K. Panskikh, "Metod khrupkikh tenzochuvstvitelnykh pokrytiy" [Method of Brittle Strain-Sensitive Coatings], Moscow, Izdatelstvo "Nauka", 1978.

COPYRIGHT: Izdatelstvo "Nauka", "Mashinovedeniye", 1986

6521

CSO: 1861/102

## DEVELOPMENT AND INVESTIGATION OF ACTIVE PNEUMATIC VIBRATION INSULATION SYSTEMS FOR HUMAN OPERATOR

Moscow IZVESTIYA VYSSHIKH UCHEBNIKH ZAVEDENIY: MASHINOSTROYENIYE in Russian No 2, Feb 87 (manuscript received 15 Apr 86) pp 94-98

[Article by A. V. Andreychikov, assistant; first paragraph is introduction]

[Text] The results of full-scale investigations of the vibration-protection properties of three versions of new pneumatic vibration-insulation systems for the seat of the human operator with pressure stabilizer are presented. The tests of the developed systems on modern high-speed 2TE116 and 2TE121 locomotives showed high effectiveness in the region of low and high vibration frequencies.

The increase of the speeds and power of transport vehicle power plants leads to an expansion of the vibrational spectrum acting on the human operator. The problem of vibration protection of operators against low-and high-frequency vibrations of different intensity becomes especially timely in this regard.

One of the most promising methods of improving the vibration state of transport vehicle operator workstations is to use active pneumatic vibration insulation systems (connected to an external compressed air energy source). Known pneumatic vibration-protection systems [1] have relatively high natural vibration frequencies (1.6-1.8 Hz) and absolute transmission factor at resonance ( $T_A = 2-3$ ). Therefore, they provide effective protection of the human operator only at frequencies above 2.5-3 Hz, which does not meet either Soviet or international standards.

Three essentially new versions of pneumatic vibration-protection systems [2-4] for the human operator were developed and investigated to solve the indicated problem. The first version contains an operating chamber 1 (Figure 1) 390 cm<sup>3</sup> in volume, based on a double-corrugated rubber cord shell of model I-08, a damper chamber 2 0.08 cm<sup>3</sup> in volume, a jet-type reactor 3, fixed 4 and moveable 5 straps, connected to each other by parallel levers 6 and 7, the axes of which are placed in bearing seats. The seat cushion 8 is attached to the moveable clamp 5, the maximum stroke of which is  $\pm 0.07$  m. The pneumatic suspension is

supplied with a pressure stabilizer 9 for maintaining levers 4 and 5 automatically in the horizontal position regardless of the weight of the human operator, sitting on cushion 8.

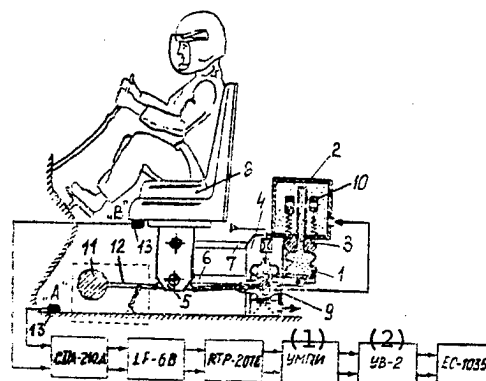


Figure 1. Schematic Structural Diagram of Active Pneumatic Vibration Insulation System With Pressure Stabilizer for Human Operator

Key:

1. Multichannel data converter controller
2. Input device

The distinguishing feature of the design of the pneumatic vibration-protection system according to version II (Figure 1) is that the operating 1 and damping 2 chambers are connected by a resonator-type throttling device, which ensures frequency-dependent inelastic resistance to the air to be compressed.

The third version of the pneumatic suspension contains an inertial element 11 and motion transducer 12.

The working principle of the indicated pneumatic vibration-insulation systems is described in [2-4], respectively. All three versions of pneumatic suspensions were investigated on 2TE116 and 2TE121 mainline diesel locomotives, moving on a test track. Accelerations during the tests were recorded in the vertical direction at two points: near the base of the seat (point A) and on the movable bracket 5 (point B) in the frequency range from 0.5 to 40 Hz using a magnetic recording system that included BWH-301 (RFT, German Democratic Republic) vibration transducers 13, DPM-6E amplifier, CDA-210A low-frequency filter and RTP-207E tape recorder (equipment of the Kiowa Company, Japan). The experimental data, recorded on magnetic tape in analog form, was converted to digital form by a multichannel data converter (UMPI) and was entered by a UB-2 input device into a YeS-1035 digital computer, on which the mean square values of vibration accelerations  $\tilde{a}_i$  ( $\text{m}\cdot\text{s}^{-2}$ ) in one-third octave frequency bands in the range from 0.8 to 40 Hz and the function of the absolute transfer factor  $T_A(f)$  were recorded by a special program and by known formulas [5].

The value of  $\tilde{a}_i$  was calculated by the spectral acceleration density function, computed by the fast Fourier transform method according to the formula

$$\tilde{a}_i = \sqrt{\int_{f_H}^{f_B} \tilde{S}(f) df}$$

where  $\tilde{S}(f)$  is estimation of the spectral acceleration density and  $f_H$  and  $f_B$  are the lower and upper frequency bounds, corresponding to the bandpass of the  $i$ -th third-octave filter.

The transfer functions  $T_A(f)$  were calculated without regard to phase relations (the absolute value) by the formula

$$T_A(f) = \sqrt{\frac{\tilde{S}_y(f)}{\tilde{S}_x(f)}}$$

where  $\tilde{S}_x(f)$  and  $\tilde{S}_y(f)$  are the estimate of the spectral acceleration density function at the input (point A) and output (point B) of the system to be tested, respectively.

The transfer functions of the absolute transfer factor  $T_A(f)$  of the developed versions of pneumatic vibration-insulation systems in the frequency range of 0.8-16 Hz are presented in Figure 2. Version I was investigated with throttle diameters 3, equal to  $d_1 = 3.0$  mm,  $d_2 = 2.0$  mm,  $d_3 = 1.5$  mm and  $d_4 = 0$  mm, respectively, curves 1, 2, 3 and 4. It is obvious from analysis of these curves that the natural vibration frequency of the human operator on a pneumatic suspension increased from 1.25 to 1.6 Hz with a decrease of throttle diameter from  $d_1 = 3.0$  mm to  $d_3 = 1.5$  mm and that the absolute transfer factor  $T_A$  decreased from 3.1 to 2.2. Curve 5 with the dashed line (Figure 2) indicates the maximum (globally optimum) frequency characteristic  $T_A(f)$  for a given type of vibration-protection pneumatic suspension. The maximum characteristic 5 can be realized by using a pneumatic suspension, having variable structure as a function of vibrational frequency.

Automatic variation of the structure of the pneumatic suspension is achieved due to the cavity-type throttle (version II) [3].

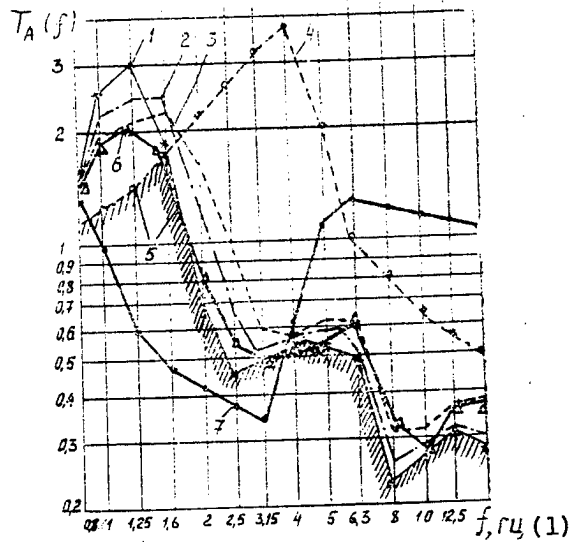


Figure 2. Transfer Functions of Absolute Transfer Factor  $T_A(f)$

Key:

1. Hz

A pneumatic suspension with cavity-type throttle (version II) makes it possible to reduce the absolute transfer factor  $T_A$  on the natural vibrational frequency of the pneumatic suspension  $f_0 = 1.25$  Hz to 2.0 (curve 6, Figure 2). At the same time, a pneumatic suspension on resonant frequencies does not differ in vibration-insulating properties according to version II from the vibration-protection system with zero damping (curve 1, Figure 2). It is obvious from analysis of the transfer function  $T_A(f)$  (curves 1, 2, 3 and 6) that the latter has a second rise in the frequency range of 3.5-6.5 Hz. This confirms the conclusions that the body of the human operator behaves like a dynamic vibration damper with natural vibration frequency in the range of 4-5 Hz [1].

It was established as a result of testing the pneumatic suspension according to version III that the ratio of the arms of an additional two-arm lever of the motion conversion mechanism 12 (Figure 1) should comprise  $N_2/N_1 = 2.9$ , the mass of the inertial element 11 should comprise 9-10 kg and the diameter of the interchamber throttle should comprise 3 mm to ensure a minimum transfer function  $T_A(f)$  in the ultralow frequency range of 1.0-4.0 Hz (the frequency range with the greatest vibration intensity of most transport vehicles and the main resonances of the human body). The transfer function  $T_A(f)$  of the pneumatic suspension for version III is presented in Figure 2, curve 7.

Analysis of the mean square values of vibration accelerations in the third-octave frequency bands (Figure 3) shows that the vibration-protection properties of a pneumatic vibration-insulating system according to version II are manifested at frequencies of 1.8-2 Hz. This pneumatic suspension on the 2TE116

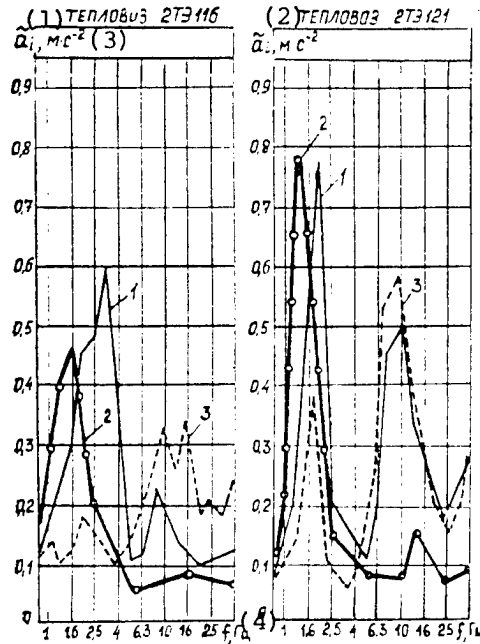


Figure 3. Mean Square Values of Vibration Accelerations in Third-Octave Frequency Bands, Recorded at Engineer Workstations of 2TE116 and 2TE121 Diesel Locomotives at Speed of 100 km/hr: 1--vibration accelerations, recorded on cushions of standard engineer seats; 2, 3--vibration accelerations recorded on movable bracket of pneumatic vibration-protection system according to versions II and III, respectively

Key:

- |                             |                     |
|-----------------------------|---------------------|
| 1. 2TE116 diesel locomotive | 3. $m \cdot s^{-2}$ |
| 2. 2TE121 diesel locomotive | 4. Hz               |

diesel locomotive permits one to "tune" the vibration-insulated object (man) from the resonant vibrational frequency of the body of the locomotive on spring suspension and to improve the vibration state of the engineer's workstation in the frequency range of 2.0-40 Hz. Tests of this version of the pneumatic suspension on the 2TE121 diesel locomotive showed that the natural vibrational frequency of the dynamic vibration-protection seat-man system essentially coincides with the resonant vibrational frequency of the body of this locomotive on spring suspension. Therefore, the amplitude value of the vibration accelerations on the seat with pneumatic suspension has a significant level at frequency of 1.25 Hz.

Investigations of the pneumatic vibration-protection seat system according to version III, conducted on 2TE116 and 2TE121 diesel locomotives, showed that it is effective in the ultralow frequency range (0.8-4 Hz) and permits one to reduce vibration on the engineer's workstation by a factor of 2.4-4.5 in the indicated frequency band.

## Conclusions

1. A pneumatic vibration-protection human operator seat system with frequency-dependent inelastic resistance can be used effectively on different transport vehicles and, specifically, on shunting and commercial locomotives, having natural vibrational frequencies of the body on spring suspension of not less than 1.6 Hz, road vehicles, wheeled tractor-cultivators, road construction machines, trucks and grain and forage harvesters.

2. A pneumatic vibration-insulation system with motion and inertial mass conversion mechanism is recommended for high-speed mainline and passenger locomotives with natural vibrational frequency of the body on spring suspension in the range of 0.8-1.6 Hz. The given vibration-protection system can also be used effectively to improve the working conditions of tractor operators and operators of special transport vehicles on tracks and drivers of passenger buses.

## BIBLIOGRAPHY

1. Kochetov, O. S., "Vibration-Protection Suspension with Nonlinear Characteristics," AVTOMOBILNAYA PROMYSHLENNOST, No 7, 1984.
2. Andreychikov, A. V., et al., "Pneumatic Springs," USSR Inventor's Certificate No. 1161736, F16 F9/04, BYULLETEN IZOBRETENIY, No 22, 1985.
3. Andreychikov, A. V., et al., "Pneumatic Flexible Suspension Element for Transport Vehicle," USSR Inventor's Certificate No. 954261, B60 G11/26, BYULLETEN IZOBRETENIY, No 32, 1982.
4. Andreychikov, A. V., et al., "Seat Suspension of Transport Vehicle," USSR Inventor's Certificate No. 1138336, B60 N1/02, BYULLETEN IZOBRETENIY, No 5, 1985.
5. Bendat, J., and A. Peersoll, "Izmereniye i analiz sluchaynykh protsessov" [Measurement and Analysis of Random Processes], Moscow, 1974.

COPYRIGHT: "IZVESTIYA VUZOV. MASHINOSTROYENIYE"

6521

CSO: 1861/145

## APPLICATION OF AIR MICROEJECTOR IN VACUUM GRIPPING DEVICE OF INDUSTRIAL ROBOT

Moscow MEKHANIZATSIYA I AVTOMATIZATSIYA PROIZVODSTVA in Russian No 12, Dec 86  
p 25

[Article by N.P. Zaporozhets, engineer]

[Text] Calculation (optimization) of the principal geometrical and dynamic parameters of an air microejector is a rather complicated process. Therefore, the organization of experiments with an air microejector for purposes of accumulating experimental data is justified.

A line diagram of a vacuum gripping device based on an air microejector with the ejecting stream fed peripherally is presented in fig 1. In association with the inevitability of leaks originating between the suction device and the surface of the part, it is suggested that atmospheric air be drawn in and ejected into the atmosphere again.

The relationship between the degree of vacuum and the air microejector's parameters can be represented as follows:

$$\Delta P_v/P_n = f(\Pi_0, \alpha, \bar{L}), \quad (1)$$

where  $\Delta P_v$  is the degree of vacuum;  $\Pi_0 = P_{01}/P_n$  is the relative differential of available pressures;  $\alpha = F_1/F_2$  is the microejector's principal geometrical parameter; and  $\bar{L} = L_{ks}/d_{ks}$  is the relative length of the mixing chamber (here  $P_{01}$  is the total pressure of the ejecting stream,  $P_n$  is the ambient pressure,  $F_1$  and  $F_2$  are the areas of the outlet sections of the nozzles for the ejecting and the ejected streams,  $L_{ks}$  is the length of the mixing chamber and  $d_{ks}$  is the diameter of the cylindrical mixing chamber).

It follows from expression (1) that the degree of vacuum is a complex function of dynamical and geometrical parameters of the air microejector. In addition, parameters  $\Pi_0$ ,  $\alpha$  and  $L$  are interrelated.

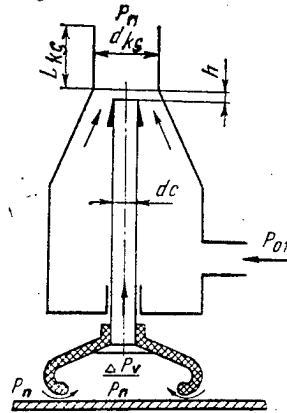


Figure 1. Sketch of Vacuum Gripping Device Based on Air Microejector

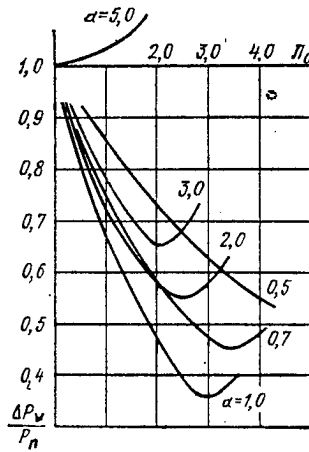


Figure 2. Dependence of Degree of Vacuum,  $\Delta P_v/P_n$ , on Pressure Differential,  $\Pi_0$ , with Various Values of Microejector's Principal Geometrical Parameter,

Let us take as independent parameters the combination of the dynamical parameter,  $\Pi_0$ , and one of the geometrical parameters ( $\alpha$  or  $\bar{L}$ ) with a fixed value of the other one. Then general equation (1) can be represented by particular expressions of it:

$$\Delta P_v/P_n = f_1(\Pi_0, \alpha); \quad (2)$$

$$\Delta P_v/P_n = f_2(\Pi_0, \bar{L}). \quad (3)$$

Experimental curves describing relationship (2), are presented in fig 2. The influence of parameter  $\Pi_0$  on the degree of vacuum is not only considerable, but also unique. Extreme values of the vacuum have been detected for various values of the principal geometrical parameter.

Experiments were performed with the following values:  $d_s$  (nozzle diameter) = 4 mm,  $d_{ks} = 6$  mm and  $L_{ks} = 30$  mm.

The principal geometrical parameter,  $\alpha$ , varied on account of variation in the size of the gap,  $h$ , (cf. fig 1) between the outlet section of the nozzle for the ejecting stream and the beginning section of the mixing chamber. The value of  $\Pi_0$  varied over the range of the pressure of the plant's air supply system.

With an increase in  $\Pi_0$ , the size of the vacuum increases and reaches a maximum value for the optimal geometry, with  $h = 0$  and  $\Pi_{0,opt} = 3$ .

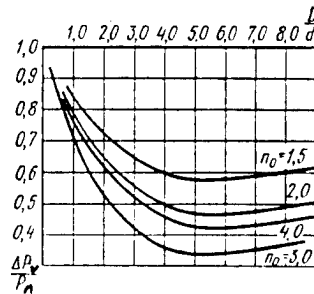


Figure 3. Dependence of Size of Vacuum,  $\Delta P_v/P_n$ , on Relative Length,  $\bar{L}$ , of Microinjector's Mixing Chamber

Experimental curves defining the relationship between the size of the vacuum and the relative length of the mixing chamber are presented in fig 3. It is obvious from these curves that the optimal relative length of the microinjector's mixing chamber is  $\bar{L}_{opt} \sim 5$ .

The results obtained make it possible to optimize the principal parameters of an air microinjector with the ejecting stream fed peripherally.

The results of these studies can be recommended for practical application.

COPYRIGHT: Izdatelstvo "Mashinostroyeniye", "Mekhanizatsiya i avtomatizatsiya proizvodstva", 1986

8831

CSO: 1861/154

## ANALYSIS OF POSSIBILITY AND EFFECTIVENESS OF USING COMPOSITE MATERIALS IN GRAIN COMBINES TO REDUCE WEIGHT

Moscow MASHINOVEDENIYE in Russian No 6, Nov-Dec 86 (manuscript received 22 Apr 86) pp 90-93

[Article by A. V. Berezin, V. G. Lyutsau, Yu. A. Babin, Yu. F. Klimchuk and S. K. Abramov, Moscow and Rostov-na-Donu]

[Text] The possibility and effectiveness of using composite materials in grain combine designs were analyzed in the preliminary design stage. A general estimate of using composite materials requires a knowledge of the stress-strain state of the structure for standard operating loads using safety factors, the presence of overloads and the service life of the products. We note that experience in design of aircraft structures from composites has now been accumulated [1] and a corresponding analysis of the possibility and effectiveness of using composites in the structure of harvest combines was made in regard to this.

The most widely used of composites with polymer matrix are now glass fiber-reinforced plastics, carbon fiber-reinforced plastics and organic fiber-reinforced plastics. These materials have become widespread. They have a sufficiently well-developed technology, stable properties and rather high weight efficiency. The densities of these types of composites have the following values: glass fiber-reinforced plastics have 1.9-2 g/cm<sup>3</sup>, carbon fiber-reinforced plastics have 1.45-1.6 g/cm<sup>3</sup> and organic fiber-reinforced plastics have 1.2 g/cm<sup>3</sup>, respectively. The most promising composites which can be used in the structure of harvest combines are organic fiber-reinforced and glass fiber-reinforced plastics. Organic fiber-reinforced plastics are preferable from the viewpoint of their higher weight efficiency for those assemblies and structures where compressive force flows are low or are absent. Carbon fiber-reinforced plastics must be used with extreme care in designs of agricultural machines, since they have low failure strains upon loading in the direction of the fiber ( $\epsilon_{\max} \sim 0.6$  percent) and very low impact strength, which characterizes the operational suitability of structures of the given material. The puncture values of composite materials and of some metallic sheet materials 1 mm thick with a sphere 6.37 mm in diameter are presented in Table 1. The low puncture

values result in the fact that slight effects cause damage to the material and, accordingly, reduce the strength and durability of the structure. The energy required to pierce modern structural carbon fiber-reinforced plastics is an order less than the energy of piercing light alloys of type D-16 and VT-20 [2, 3]. It is obvious from Table 1 that organic fiber-reinforced and glass fiber-reinforced plastics have piercing values of the same order as that of light alloys and also have greater failure strains compared to carbon fiber-reinforced plastics. Specifically, the failure strains of organic fiber-reinforced plastics comprise 2-5 percent.

Table 1

Material	Energy J
VT-20 titanium alloy	35
D-16T aluminum alloy	17
Organic fiber-reinforced plastic	13
Glass fiber-reinforced plastic	10
Carbon fiber-reinforced plastic	2

Let us consider the possibility of using composite materials in the unloaded part of the structure. These structural elements include the covers of the combine, hopper, straw collector, surrounding panels, covers of the air intake and of the cab. One can ensure beforehand the efficiency and high reliability with appreciable reduction of the weight of the combine for these structural elements, if strength and bending stiffness conditions of the metal version are retained in the composite version.

The most widely used procedure of creating high stiffness in the cover structures is to use structures with a filler [4, 5]. Let us consider the possibility of using them in the elements of grain combines. Since there is uncertainty of the force flows and also variability of them during operation and through the area of the elements, it is rational to select the placement of composite materials as isotropic, i.e., placement of  $[0/\pm 60]$ . It is sufficient to make the skins of honeycomb panels three-ply with regard to the high strength of organic fiber-reinforced plastic ( $\sigma_b = 15 \cdot 10^2$  MPa). The thickness of a single layer of SVM organic fiber-reinforced plastic comprises 0.15 mm and, accordingly, the thickness of the skin is 0.45 mm. The skin of grain combines is made from sheet steel 1.5 mm thick with Young's modulus of  $E = 2 \cdot 10^5$  MPa and  $\sigma_{-1} \sim 100$  MPa with regard to service life and concentration in the weld seams. Accordingly, the cylindrical stiffness of a metal panel will be  $D_{\pi\pi} = 2E[\delta^3/3 (1 - \nu^2)] = 5.6 \cdot 10^4$  MPa $\cdot$ mm<sup>3</sup>, where  $2\delta = 1.5$  mm is the thickness of the sheet.

The cylindrical stiffness of a panel with filler is calculated by the formula [6]

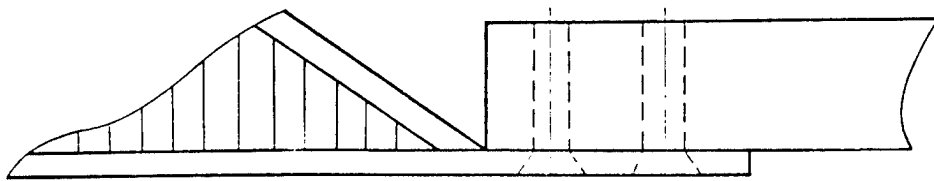
$$D_{\text{ext}} = \frac{2E\delta_1}{(1-\nu^2)} \left[ \frac{\delta_1^2}{12} + \left( h + \frac{\delta_1}{2} \right)^2 \right],$$

where  $\delta_1$  is the thickness of the outer layer,  $2h$  is the thickness of the filler,  $E$  is Young's modulus and  $\nu$  is Poisson's coefficient.

The elastic characteristics of the single layer of SVM organic fiber-reinforced plastic have the following values [7]:  $E_{11} = 6 \cdot 10^4$  MPa,  $E_{22} = 4 \cdot 10^4$  MPa,  $G_{12} = 1.8 \cdot 10^3$  MPa and  $\nu_{12} = 0.3$ .

The use of the standard method of calculating the elastic characteristics of a laminated composite [8] permits one to determine the moduli of elasticity, which will be  $E_x = E_y = 3 \cdot 10^4$  MPa and  $G_{xy} = 10^4$  MPa for placement of  $[0/\pm 60]$ . By equalizing the cylindrical stiffnesses of a metal and composite product, we find that the thickness of the filler will be  $2h \approx 2.4$  mm at  $\delta_1 = 0.45$  mm. The total thickness of the panels will be equal to 3.3 mm in this case and the cylindrical stiffness remains the same as that of a metal skin. Spheroplasts, filled with foam plastics, can be used as fillers. In the latter case, the specific weight of the filler is equal to  $\rho_1 = 0.4$  g/cm<sup>3</sup>. It should be noted that the tensile stiffness in the plane of the sheet decreases and if necessary, one should use constructive measures to ensure the stiffness in the plane of the sheet. Stringer sets of reinforcing cover plates, which are made from high-modulus composites [9], are used for these purposes. The use of glued joints of the stringers to the skins of the panels is possible. Naturally, this measure results in an increase of the weight of the structure. Since it is known that the skin is unloaded, only the version with retained bending stiffness is considered. There are very large strength margins in this version, which makes it possible to disregard the decrease of pliancy in the plane of the sheet. The tensile strength of SVM organic fiber-reinforced plastic is  $\sigma_{11} = 1.5 \cdot 10^3$  MPa along the fiber and  $\sigma_{22} \sim 22$  MPa at right angles to the fiber. Analysis of the limiting surfaces of disoriented composites with placement of  $[0/\pm 60]$  shows [10] that the minimum strength is  $\sigma_{-1} \approx 3.5 \cdot 10^2$  MPa with regard to life based on  $10^6$  cycles for arbitrary orientation of the force flow to the direction of the fiber in any of the layers of the composite. Therefore, the maximum force flows for panels with SVM organic fiber-reinforced plastic skins with skin thickness of 0.45 mm will be  $F_{\text{K}}^* = 3.15 \cdot 10^2$  MPa·mm. Accordingly, the maximum force flows for metal panels with skin thickness of 1.5 mm are equal to  $F_{\text{K}}^* = 1.5 \cdot 10^2$  MPa·mm and the strength reserves in composite skins are twofold greater than those of metal skins. It should also be noted that the effective coefficient of stress concentration of SVM organic fiber-reinforced plastic does not exceed 1.5, whereas that of metal versions reaches 3.

Let us now consider the problem of the points of attachment and connection of composite materials. Lacing with wire (so-called point connections) is now a rather widespread method of joining. It ensures strength of the joint, equal to that of the basic material. Another method of attachment is the use of bolted connections, especially for metal-composite systems.



The structure of the points of attaching honeycomb panels to metal elements of the structure is shown in the figure. It is shown that this design is more efficient from the viewpoint of fatigue strength and load ratio.

The bearing strength of organic fiber-reinforced plastic is higher than that of carbon fiber-reinforced plastics with the same reinforcing scheme. Therefore,  $\sigma_{-1}^o > 2 \cdot 10^2$  MPa, where  $\sigma_{-1}^o$  is the bearing strength, in bolted connections for organic fiber-reinforced plastic with reinforcing scheme  $[0/\pm 60]$  and with regard to the results of fatigue tests based on  $10^6$  cycles. The equal strength of bolted connections will be fulfilled if the distance between bolts is selected by the formula  $b = 1.4d$ , where  $d$  is the diameter of the bolt.

Table 2

(1) Наименование конструкции	(2) Масса металли- ческого варианта, кг	(3) Масса композитных вариантов, кг			(4) Экономия массы, кг		
		1	2	3	1	2	3
(5) Ограждающие панели 2 шт.	70	6.4	12.2	35	63	57.8	35
(6) Обшивки коробки воз- духзаборника	85	8	16	42.5	77	69	42.5
(7) Верхняя крышка каби- ны	30	3	5.8	15	27	24.2	15
(8) Панели копнителя	94	7	13.5	47	87	78.5	47
(9) Бункер	800	150	288	400	650	512	400
(10) Обшивка комбайна	1500	120	230	750	1380	1270	750
(11) Заполнитель	-	217	217	-	-	-	-
(12) Всего	2580	521.4	784.5	1294.5	2077	1804	1294.5

Key:

- |                                     |                           |
|-------------------------------------|---------------------------|
| 1. Name of structure                | 7. Upper cab cover        |
| 2. Weight of metal version, kg      | 8. Straw collector panels |
| 3. Weight of composite versions, kg | 9. Hopper                 |
| 4. Saving of weight, kg             | 10. Skin of combine       |
| 5. Enclosing panels, 2 units        | 11. Filler                |
| 6. Coverings of air intake boxes    | 12. Total                 |

Based on the foregoing, the reduction of the weight of the composite version of the design was estimated. The results of calculation when using organic fiber-reinforced plastic are presented in columns 3 and 4 under number 1 (Table 2). Estimation of the effectiveness of using glass fiber-reinforced plastic with elastic and strength characteristics for a single layer ( $E_{11} = 4.5 \cdot 10^4$  MPa,  $E_{22} = 1.5 \cdot 10^4$  MPa,  $G_{12} = 0.79 \cdot 10^4$  MPa,  $\nu_{12} = 0.3$ ,  $\sigma_{11}^P = 1.2 \cdot 10^3$  MPa,  $\sigma_{11}^{C*} = 0.64 \cdot 10^3$  MPa,  $\sigma_{22}^P = 0.4 \cdot 10^2$  MPa,  $\sigma_{22}^{C*} = 0.7 \cdot 10^2$  MPa and  $\tau = 0.6 \cdot 10^2$  MPa) leads to a 1.92-fold increase of the weight of composites compared to structural elements made of organic fiber-reinforced plastic, while retaining the strength and fatigue characteristics. This increase is achieved due to the need to make the skins thicker and due to the fact that the specific weight of glass fiber-reinforced plastic is greater than the specific weight of organic fiber-reinforced plastic. Accordingly, the results of calculating the weight of glass fiber-reinforced plastic structural elements of grain combines and the saving of weight compared to the metal version are presented in columns 3 and 4 under number 2.

Let us now consider the use of one-ply rather than three-ply structures. Again let us use the equality of the cylindrical stiffnesses of the metal and composite version of skin structures as the criterion of comparison. Let us consider the glass fiber-reinforced plastic version with modulus of elasticity of  $E = 2.5 \cdot 10^4$  MPa. We find from the condition of equal stiffness that the thickness of the skin in the glass fiber-reinforced plastic one-ply version is equal to  $2\delta = 3$  mm. Accordingly, the results of calculating the mass of a one-ply glass fiber-reinforced plastic version and the saving of weight compared to the metal version are presented in columns 3 and 4 (Table 2).

It follows from the results of Table 2 that the use of organic fiber-reinforced plastic structures with filler may yield the greatest weight savings. The use of one-ply glass fiber-reinforced plastic materials without filler has the lowest efficiency. It should be noted that the use of thicker composite sheets leads to an increase of the piercing energy and the structure becomes less sensitive to damage. It should also be noted that a reduction of the weight of grain combines by using composite materials in the structure leads to a decrease of fuel consumption. We note the high corrosion resistance of composite materials and also a decrease of pressure on the soil and other positive effects due to using them in combine structures.

It must also be taken into account that the use of composite materials as strengthening elements for a steel framework structure is inefficient, since the moduli of elasticity do not exceed those of steels and the metal part of the structure is not unloaded due to redistribution of stresses through the cross section.

The most advantageous from the viewpoint of economy is the use of glass fiber-reinforced panels with filler, although this measure also results in a lower decrease of structural weight of grain combines than the use of organic fiber-reinforced plastic.

## BIBLIOGRAPHY

1. Rabotnov, Yu. N., A. A. Tupolev, V. F. Kutinov, V. P. Kogayev, A. V. Berezin et al., "Use of Carbon Fiber-Reinforced Plastics in Aircraft Design," MEKHANIKA KOMPOZITNYKH MATERIALOV, No 4, 1981.
2. Dudka, K. K., I. N. Preobrazhenskiy and A. S. Shestakov, "One of the Approaches to Estimation of the Impact Strength of Carbon Fiber-Reinforced Plastic," MEKHANIKA KOMPOZITNYKH MATERIALOV, No 4, 1983.
3. Muzychenko, V. P., and V. I. Postnov, "On the Possibility of Predicting the Resistance of Metal Alloys to Piercing," ZHURNAL PRIKLADNOY MEKHANIKI I TEKHNICHESKOY FIZIKI, No 5, 1984.
4. Yeger, S. M., "Proyektirovaniye passazhirskikh reaktivnykh samoletov" [Design of Jet Passenger Aircraft], Moscow, Izdatelstvo "Mashinostroyeniye", 1966.
5. Kan, S. M., and I. A. Sverdlov, "Raschet samoleta na prochnost" [Strength Calculation of Aircraft], Moscow, Izdatelstvo "Mashinostroyeniye", 1966.
6. Aleksandrov, A. Ya., L. E. Bryukker, L. M. Kurshinet al., "Raschet trekhsloynnykh paneley" [Calculation of Three-Ply Panels], Moscow, Oborongiz, 1960.
7. Plume, E. Z., Ye. A. Sokolov and R. D. Maksimov, "Predicting the Characteristics of Elasticity of Organic Fiber-Reinforced Plastic by the Properties of Their Structural Components," PROBLEMY PROCHNOSTI, No 2, 1980.
8. Rowlands, R., "Flow and Loss of Supporting Power of Composites Under Conditions of Two-Axial Stress State: Comparison of Calculation and Experimental Data," in "Neuprugkiye svoystva kompozitsionnykh materialov" [Inelastic Properties of Composite Materials], Moscow, Izdatelstvo "Mir", 1978.
9. Bert, C., "Calculation of Plates," in "Analiz i proyektirovaniye konstruktsiy" [Analysis and Design of Structures], Vol 7, Moscow, Izdatelstvo "Mashinostroyeniye", 1978.
10. Oldyrev, P. P., and R. A. Apinis, "On the Effect of Loading Frequency on Low-Cycle Fatigue of Organic Fiber-Reinforced Plastic," MEKHANIKA KOMPOZITNYKH MATERIALOV, No 4, 1983.

COPYRIGHT: Izdatelstvo: "Nauka", "Mashinovedeniye", 1986

6521

CSO: 1861/100

## NEW MACHINE TOOL PRODUCTS AT NTP'86

Moscow MEKHANIZATSIYA I AVTOMATIZATSIYA PROIZVODSTVA in Russian No 9, Sep 86 pp 26-32 [Continuation of reports from Nos 7 and 8 of this journal]

[Text] The set of robotization devices for metalworking equipment (Figure 1) is designed to load lathe-type machine tools with parts of the shaft-flange type. The given set can be used to service other types of machine tools and also press equipment. The set consists of a SM40Ts4011 robot and two ball storage conveyers.

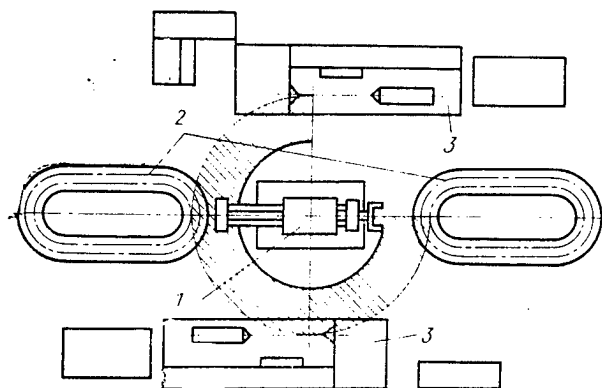


Figure 1: Set of Robotization Devices: 1--robot; 2--storage conveyers; 3--machine tools

The PR [industrial robot] is one-armed with five degrees of freedom (without movement of the gripper). The drive is hydraulic and the hydraulic station is built into the base of the robot.

The ball storage conveyer is designed on the modular principle. The transport distance and configuration of the conveyer are dependent on the number and type of required modules.

## Specifications of Set

### Robot:

number of machine tools to be serviced	2
load capacity, kg	40
precision of positioning, mm	±1.5
least distance from bottom of base to axis of holding device, mm	1,060
control system	Cyclic
controller	UTsM-663
weight, kg	1,100

### Storage conveyer:

type of drive	Electric
number of trays to be installed	up to 15
speed of trays, mm/s	50-1,000
accuracy of positioning trays, mm	±1.0

The developer is PKBplastmash and the manufacturer is the Experimental Design PKBplastmash, Krasnodar.

The KhShK-001 grinding system (Figure 2) is designed for outside grinding of smooth and discontinuous cylindrical tapered and end surfaces of stepped shafts in the automatic cycle.

The system includes a semi-automatic round grinding machine with numerical program control, a KhShR-001-1 industrial robot with numerical program control and a KhShK-001.400 holder.

Cylindrical, end and tapered surfaces are machined according to a given program. Tapered surfaces are ground by rotation of the top table at a given angle.

The abrasive disk is adjusted automatically around the periphery with a diamond pencil, mounted in a special holder attached to the body of the rear chuck.

The floor-mounted robot takes the part from the storage holder, installs it on the center line of the machine tool and inserts it into the chuck. After machining one half of the part, the robot removes the part from the center line of the machine tool, raises it, turns it by 180° and installs it in the machine tool for machining the second half of the part. The part is returned to the storage device after the part is completely machined.

The robot has three wide-range quickly removable self-centering grippers, which hold stepped shafts from 25-200 mm in diameter. The time required to change the grippers is no more than 1 minute. With software, the grippers are changed automatically. Equipping the robot with wide-range grippers and center chuck makes it possible to expend no more than 30-40 min to readjust for a different product.

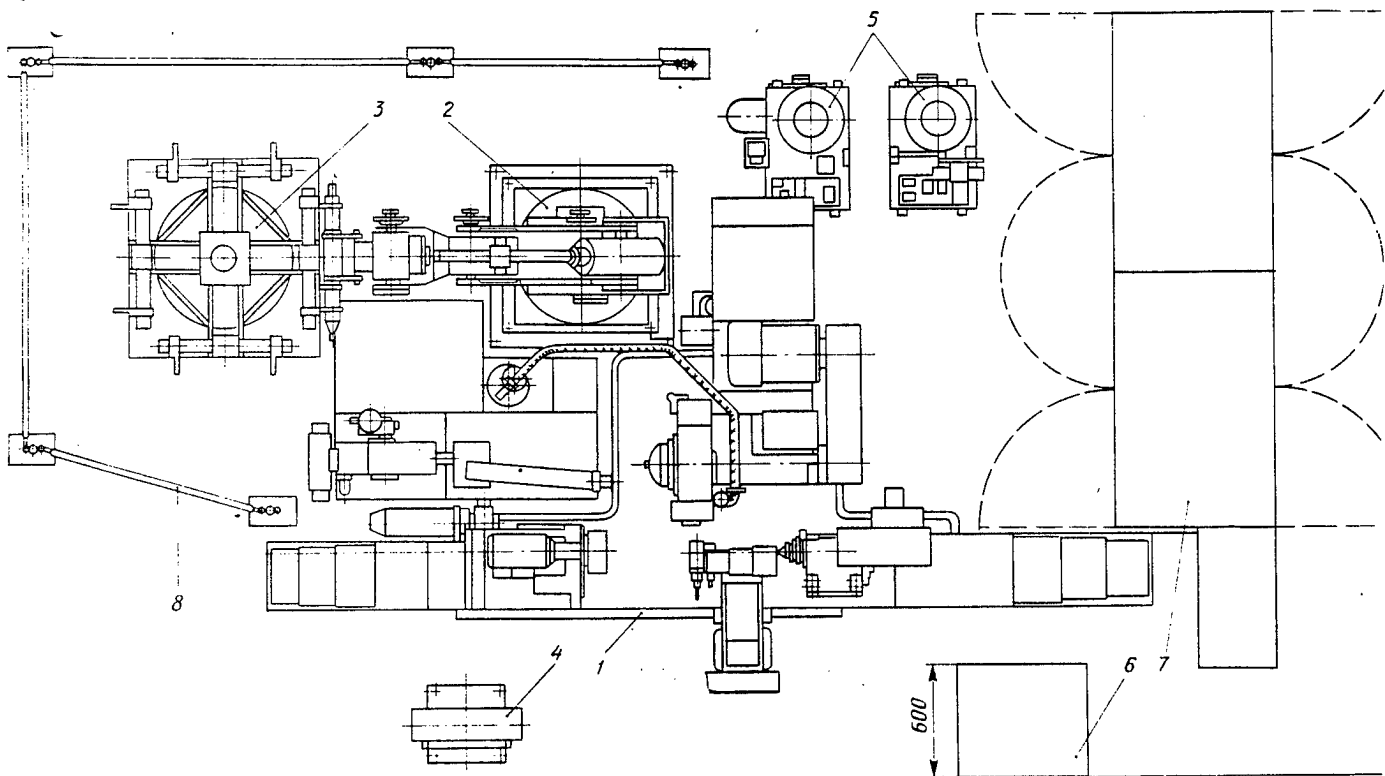


Figure 2. KhShK-001 Grinding System: 1--machine tool; 2--robot; 3--holder; 4--robot control console; 5--hydraulic module; 6--numerical program controller; 7--electric cabinet; 8--guard rail

The machine tool and robot are controlled from a numerical program controller based on a microcomputer with software, developed by the Kharkov SPO [Machine Tool Production Association imeni S. V. Kosior].

Model 2M32 numerical program controller is used for the machine tool and model 2R32 controller is used for the robot. The control program is entered from papertape through a photoreader or from the operator's consoles into the machine tool and robot for machining a specific part.

The storage holder has four removable trays for 8-20 parts each and supports the operation of the module for 8 hours. The floor-type robot with five degrees of freedom services two machine tools.

#### Precision Parameters of Machining

Constant Diameter in longitudinal section, mm	0.002
Roundness, mm	0.001
Play of end surfaces on radius of 45 mm, mm	0.004
Smoothness of end surfaces, mm	0.004
Roughness of surface to be machined Ra, $\mu\text{m}$	0.10

### Specifications of System

Greatest dimensions of product to be installed, mm:		
diameter		260
length		710
Greatest weight of product to be installed, kg		55
Robot servicing zone, mm:		
radius		525-2,140
height		26-3,300
Number of parts loaded in holder (at diameter of 20-100 mm and length of 250-710 mm)		28-80
Type of current		Alternating three- phase
Voltage, V		380
Total power of electric motors and of electric drive of system, kW		20, 23
Overall dimensions of system, mm	7,690 x 3,860 x 3,300	
Area, m <sup>2</sup>		29, 68
Weight of system, kg		12,500

The manufacturer is the Kharkov Machine Tool Production Association imeni S.V. Kosior.

The VZ-219K system (Figure 3) is designed for sharpening and lapping headpiece end mills with abrasive and diamond disks.

The material of the cutting part of the mills to be sharpened is a solid alloy, cermet, tool or high-speed steel.

The system can be used in sharpening and resharpening of end mills at enterprises of the metalworking industry and also at tool plants.

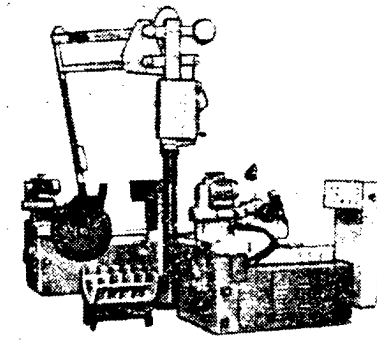


Figure 3. VZ-219K Semi-Automatic Sharpening System

## Specifications of VS-219K System

Diameter of cutters to be sharpened, mm	80-630
Number of teeth	4-90
Diameter of abrasive disk, mm	150
Rotational frequency of spindle, $\text{min}^{-1}$ :	
of abrasive disk	1,800, 3,600
of product (continuously variable), m/min	0.5-10
Power of abrasive disk drive, kW	2.5
Transverse feed, mm/revolution	0.005-0.12
Speed of controlling diamond (continuously variable), m/min	1.0-2.5
Load capacity of manipulator, including weight of holder, kg	125
Service zone of manipulator, mm:	
in height	30-1,865
in radius	400-2,310
Rotation of manipulator about column axis	Unlimited
Air pressure in pneumatic system, MPa, not less than	0.5
Force of moving part, N, not more than:	
along vertical	40
along horizontal	20
Overall dimensions of system, mm	4,000 x 3,200 x 3,095
Weight, kg	5,100

The developer is the Vitebsk Special Design Office of Gear-Machining Grinding and Sharpening Machine Tools.

The robot engineering system, designed by the Odessa Special Design Office of Diamond-Boring and Radial-Drilling Machine Tools (SKB ARS) and manufactured by the Odessa Radial-Drilling Machine Tool Plant imeni V. I. Lenin, is designed for final boring of housing parts.

The system consists of a special finishing-boring machine tool, automatic two-arm gantry-type robot and holder for installation of parts in the oriented position.

The loading and unloading arms of the robot load the machine tool with the parts to be machined from the holder and place the parts in the cells of the holder after machining. Labor productivity increased 1.5-fold due to automation of loading (unloading).

The reliability of the system is increased considerably due to heat treatment of the guide tables, an automatic centralized lubrication system, the use of a table-cleaning device and chip guides.

## Specifications of System

Number of parts to be machined simultaneously	2
Operating feed, mm/min	6-800
Fast speed, mm/min	7,000
Total power of electric motors installed in system, kW	19.3
Load capacity of each arm, kg	40
Dimensions of portal, mm:	
length	6,800
height	2,700
Stroke of arm, mm	600
Loading and unloading time (not overlapping), min	0.3
Positioning accuracy, mm	±0.5
Capacity of holder, units	48
Overall dimensions of system, mm	7,400 x 4,050 x 4,100
Weight of system, kg	12,200

The KhShR-001 industrial robot is an electromechanical floor-type robot and is designed to service round grinding tools. The robot performs the following operations: it transports blanks from storage bins to the machine tool, installs them in the machine tool and removes and transports them to storage bins of already finished shaft-type parts after machining on the machine tool.

The diameter of the blanks or parts can be from 30 to 200 mm; therefore, the robot is supplied with quickly removable grippers (Figure 4).

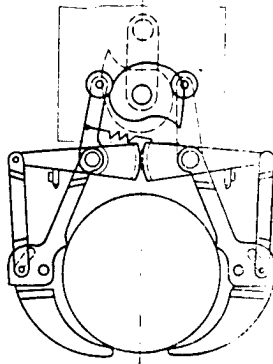


Figure 4. Structural Layout of Gripper of KhShR-001 Industrial Robot

The robot can transport parts weighing up to 63 kg at nominal speed of 1 m/s. The weight of the product to be machined can be increased to 70 kg with a decrease of rated speed by 25 percent.

The storage bins for blanks or for finished products can be both mechanized (for example, a conveyer or holders) and in the form of chutes and multilevel rotary holders.

The robot operates in an angular coordinate system and completes motions both in the horizontal and vertical and in other planes.

The robot is controlled from a pneumatic system and from an NC system, which support operation of the robot in automatic mode and monitor the entire cycle on a display, and which also support high positioning accuracy. The robot is supplied with a guard rail that limits access to the work envelope and is supplied with emergency switches.

When power is cut off, clamping the product and holding the robot arm in a fixed position are guaranteed by a self-braking worm gear and by brakes built into the electric motors of the drives.

The robot can be used in serial and large-series plants and also when servicing circular grinding and other machine tools. The robot can be used for welding, painting, cleaning weld seams and burrs and so on if it is equipped with the corresponding units.

The robot operates jointly with the machine tool in the following manner. After the switch on the main control console is set to the position "Joint operation" (operation of the robot and machine tool), after the button "Automatic operating mode" on the NC unit on the console has been switched on and after the buttons "Control circuit on" and "Start program" on the control console have been pressed, operation of the robot in the automatic mode begins. The manipulator with open grippers, located in the horizontal position, moves toward the storage bin--holder--in which the blanks are placed. The product is then clamped and the manipulator and blank move away from the holder. The gripper then rotates in the vertical plane and a command is given to transfer the blank to the machine tool.

The trajectory of the blank is in three coordinates. When the robot arm is at the level of the centers of the machine tool, the robot inserts the blank into a chuck, first centering it. After the command to clamp the blank in the machine tool has been delivered, the command to release the grippers is given and to raise the robot arm with open grippers to a specific height, where the arm will remain until machining of the part has been completed.

At the end of grinding the part, the arm with open gripper is lowered to the article and is clamped. After removing the center, the robot arm removes the part from the chuck of the machine tool and transfers the finished part to the storage bins--holders. The robot can place the finished part in its previous position or can place it in the holder for finished parts.

#### Specifications of Robot

Rated load capacity, kg	63
Dimensions of work envelope, m <sup>3</sup>	25

[Specifications of Robot continued.]

Overhang of arm from floor, mm:	
vertical	3,300
horizontal	2,140
Rated speed of actuating members, m/s	1
Indices of degrees of mobility, degrees:	
rotation of arm	270
raising (lowering) of arm	90
raising (lowering) of gripper	90
raising (lowering) of forearm	110
rotation of gripper with respect to longitudinal axis	180
Number of programmable movements (rotation of arm, raising-lowering of arm, raising-lowering of forearm)	3
Diameter of product, mm:	
least	30
greatest	200
Clamping force, N	2,500
Drive	Electromechanical
Weight of robot, kg, not more than	1,850

The KhShR-001 robot is a joint development of the Kharkov Machine Tool Production Association imeni S. V. Kosior and the Kharkov Polytechnical Institute.

The automated transport-warehouse system (ATSS) is designed for receiving, storage and delivery of blanks, semifinished products, tools and accessories to machine tools and return.

The transport system services a section consisting of seven robotized NC production complexes and also control systems: remote--with supervisor console--and automatic--from a computer.

The advantage of the given automated transport-warehouse system is the capability of direct loading of intermediate tables of metalcutting machine tools with blanks of the flange type up to 500 mm in diameter, laid in special containers, from which an industrial robot automatically loads (unloads) parts into the machine tool, and also automatically delivers tools and accessories.

The automatic transport-warehouse system and robot system provide total automation of transport and metalworking operations.

The system was introduced at the Sverdlovsk Transport Machine-Building Plant imeni Sverdlov in 1984.

Introduction of the automatic transport-warehouse system reduced labor intensiveness by 7,000 norm-hours, freed 150 m<sup>2</sup> of production area, 90 m<sup>2</sup> service-relaxation spaces and provisionally released 12 workers.

The annual saving from introduction of the automatic transport-warehouse system at the plant is 42,000 rubles.

## Specifications of Automatic Transport-Warehouse System

Packaging	Special container
Dimensions of packaging in plan, mm	600 x 800
Load capacity, kg	500
Number:	
of bins in warehouse	180
of addresses along horizontal	45
of bins along vertical	4
Greatest number of double cycles (remove-deliver) per shift	200

The developer was the NPO [Scientific Production Association] Orgstankinprom.

The manufacturers are the Ryzan SPO [Special Production Association] and the Sverdlovsk Transport Machine-Building Plant imeni Sverdlov.

Articulated balance arm manipulators (ShBM ML160.48.01) are used in those cases when the basic production equipment has no previously assigned operating program or when the position of the load is indefinite. The articulated balance-arm manipulator intensifies and copies the motion of the operator's arm, is structurally simple and has rather high precision.

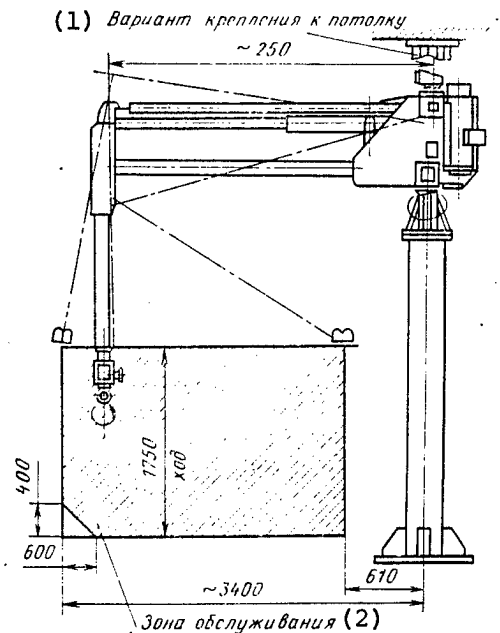


Figure 5. ML160.48.01 Articulated Balance-Arm Manipulator

Key:

1. Version of attachment to ceiling      2. Service zone

The manipulator (Figure 5) consists of an open lever-type multisection cantilever mechanism, to the end of which is mounted a control console with removable clamps. The manipulator is mounted on a column and is supplied with a hook in the basic version. The controllable electric drive raises and lowers the clamp and load. Other movements of the clamp are manual by the operator.

Special interlocking is provided--in case of sudden loss of electric power, the manipulator and load are automatically braked and stopped.

The articulated balance-arm manipulator is used widely in different plants when loading blanks into machine tools and in removal of parts, assembly of machines and units, reloading products from one transport unit to another after completion of operations, in bench assembly of serial machine tools and machines and warehouses and packing and storage sections are being equipped with them. It can also be used successfully in agriculture and in the construction industry.

The articulated balance-arm manipulator is used in foundry practice in installation and removal of molds from molding machines, in assembly of molds for loading castings into cleaning drums, in installation and removal of three-dimensional turning castings, in installation of rods and removal of castings from chill machines and so on.

The articulated balance-arm manipulator is delivered with two types of universal gripper accessories--for transport of a load with round cross section 50-100 mm in diameter and a clip clamp for transport of castings, rods and so on.

Depending on production conditions, the articulated balance-arm manipulator can be installed stationary or can be mounted on a truck, motorized and electric cart, drive carriage, on a wall, on a column, can be attached to the ceiling and so on.

#### Specifications of Articulated Balance-Arm Manipulator

Rated load capacity, kg	160
Number of degrees of mobility (without movement of clamp):	
with electric drive	1
with manual drive	3
Service radius, mm:	
greatest	3,400 ± 1.25
least	610 ± 25
Greatest vertical displacement of load clamp, mm	1,740 ± 100
Angle of rotation of manipulator about vertical axis, degrees	355 - 3
Rate of hoisting (lowering) of weight weighing, m/min:	
up to 100 kg	0.2-14
up to 160 kg	0.2-12
Speed control	stepless
Greatest overall dimensions in plan, mm	270-2,500

[Specifications of Articulated Balance-Arm Manipulator continued.]

Greatest force on lever when moving load weight 160 kg on load clamp, N	100
Weight of manipulator, kg	780
Type of power supply current	Alternating three-phase
Number of electric motors	1
Electric motor	Direct current
Power of electric motor, kW	0.85

The developers are the Scientific Research Institute of Special Casting Methods (Odessa) and the Special Design Office for Precision Casting (Tiraspol). The manufacturer is the Tiraspol Order of the October Revolution Casting Machine Plant imemi S. M. Kirov.

The 30R48 articulated balance-arm manipulator (Figure 6) is designed to mechanize hoisting-transport operations when loading production equipment of storage, mechanical assembly and electroplating plants.

The advantages of the 30R48 manipulator are: rigid grasping of load, wide continuously variable speed of raising and lowering load, convenience of control and high precision of installation of load, maintaining vertical position of axis of clamp head with any motions of lever of manipulator head and explosion safety.

A load is hoisting by pneumatic drive with the load stopped automatically at any point of the service zone and the load is moved manually in the horizontal directions.

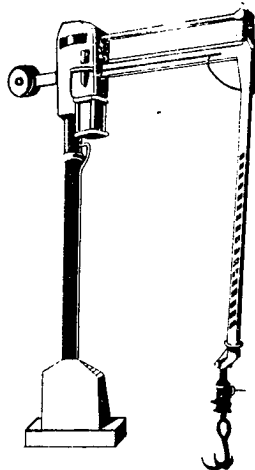


Figure 6. 30R48 Articulated Balance-Arm Manipulator

The use of the articulated balance-arm manipulator eliminates heavy physical labor in interoperations transport loading-unloading jobs and reduces the auxiliary time approximately one-half.

The annual saving is 5,500 rubles.

#### Specifications of Manipulator

Load capacity, kg	125
Service zone, m:	
in height	up to 1.6
in radius	0.4-3.0
Rate of raising load, m/s	0.05-0.3
Overall dimensions, mm	2,850 x 600 x 3,450
Weight, kg	490

The developer is VNIIP Tikhimneftemash [All-Union Scientific Research and Design Production Institute for Chemical and Petroleum Machine Building], Moscow.

Sensors developed by ENIMS [Experimental Scientific Research Institute of Metal Cutting Machines], were exhibited at the exhibition:

a DO-02 infrared detection sensor for signaling an object in the visual field of the emitter-detector system; it can also be used as a feeler element of industrial transport and assembly robots in robot production complexes or flexible manufacturing systems, specifically, to support safe functioning of equipment.

The sensor consists of an infrared light diode emitter with power indicator and photodiode detector, supplied with a status indicator.

Its working principle is based on interruption of infrared flow coming from the emitter to the detector by an object. The sensor shapes a control signal, matched to the standard input of an NC device.

The sensor retains its efficiency upon irradiation of the detector by a phonon source, located 1 m from the detector and which creates a flux of 1,000 lumens.

#### Specifications DO-02 Sensor

Effective range, m	3
Output signal (potential), V	24
Highest output current, A	0.2
Power supply voltage of DC source, V	24 <sup>+10%</sup> <sub>-15%</sub>
Consumed power (without load), V·A	1
Length of connecting cable, m	1.5
Overall dimensions, mm	63 x 25 x 21
Weight (total), kg	0.12

The DO-22 infrared sensor, which consists of an optical module that permits variation of the effective range by reducing the optical axes of the photo-emitter and photodetector and an electronics board, serves the same purpose.

Its working principle is based on detection of an infrared flux reflected by the object. The sensor is supplied with a status indicator. The DO-22 sensor retains efficiency under the same conditions as the DO-02 sensor.

#### Specifications of DO-22 Sensor

Effective range with size of object of 200 x 200 mm, m:	
unmachined aluminum	2
dark painted surface	0.5
Effective control range, m	0.15-2
Output signal (potential), V	24
Highest output current, A	0.2
Power supply voltage of DC source, V	24 <sup>+10%</sup> -15%
Consumed power (without load), V·A	1.2
Overall dimensions, mm	130 x 30 x 30
Weight, kg	0.25

Automatic lines, developed by the Sasov SKTBS and manufactured by the Sasov SPO [Special Production Organization], are designed for integrated machining of shaft and axial parts in serial, large-series and mass production.

The line is manufactured to machine a specific product. It can be manufactured by order for machining 2, 3 or more different products having identical machining process.

The set of the line includes transport-loading devices, produced by the Peoples Republic of Bulgaria, consisting of gantry-type manipulators of the Pirin type with capacity up to 10 and 40 kg, and a flexible transport system of roller conveyers with fixturing pallets.

The configuration of the arms and carriages of the gantry-type manipulator is selected as a function of the production equipment to be serviced by them with regard to reducing the parts loading (unloading) time. The parts loading (unloading) time, not combined with machining, does not exceed 10-15 s.

The presence of machined center, axial and radial holes and an active check in polishing operations are monitored on the automatic lines.

Each automatic line is equipped with a finished product counter. The lines can be supplied with the following serially manufactured metalcutting equipment: automatic milling-centering (centering-cutoff) machines, automatic hydraulic copying lathes for rough, clean and multipass (up to 8) machining and for special machining of 5-6 grooves simultaneously, automatic modular drills for

machining holes, cutting threads and milling channels and flats, automatic keyway milling machines for machining channels for prismatic and segmented keys and also for machining special channels, automatic thread machining units for milling and rolling threads, automatic slot machining units, automatic multispindle lathes, automatic boring machines for drilling deep holes and for reaming internal surfaces, automatic grinding machines for machining cylindrical and beveled surfaces, for grinding the ends and simultaneously grinding cylindrical or beveled surfaces and for centerless machining, and with NC lathes.

At the desire of the client, the automatic line can be connected to a centralized cooling and chip-removing system.

#### Specifications of Line

Diameter of part to be machined, mm:	
least	12
largest	150
Length of blank, mm:	
least	80
largest	750

The overall dimensions of the line are determined by the type and quantity of equipment contained in this line.

The automatic rotary conveyer line of model LLT-10 is designed for simultaneous manufacture of simple and complex parts from thermoplasts by the pressure casting method, for which two joint planes in the press mold are required. The press molds are located in a chain conveyor while the actuating (working) members are located in rotors.

#### Specifications of Rotary Conveyer Line

Productivity, units/min	up to 200
Volume of casting, cm <sup>3</sup>	up to 10
Specific injection pressure, MPa	up to 150
Closing force of press mold, kN	up to 160
Number of press molds	90

Compared to the best foreign and Soviet models, the line provides a four-sixfold increase of productivity, a reduction of specific power consumption by a factor of 1.5-2 and a reduction of specific metal consumption by a factor of 1.5-2.

Introduction of the line reduces labor intensiveness by a factor of 8-12, reduces the manufacturing area by a factor of 4 and releases 12-20 workers. The saving is 200,000-300,000 rubles. The return of investment of the line is 1-2 years.

A laser production system, developed by the Ivanovo SPO [Special Production Association] imeni 50-letiya SSSR is designed for automated laser hardening, heat treating and cutting and welding of parts from different materials under industrial conditions.

The association has determined a list of standard machine tool building parts and has developed machining layouts and laser process modes for flexible manufacturing conditions.

The possibility of positioning the laser beam at any point of space and of moving it along a complicated contour with high precision over a wide range of speeds provides local machining of a surface, essentially without altering its geometric dimensions. The specifics of the physicochemical processes occurring in the materials exposed to the laser emission permits one to improve the mechanical characteristics of the materials compared to other methods of machining, to cut threads, to weld various types of materials with high precision and with minimum tolerances. These operations cannot be performed by traditional methods.

Rapid readjustment of the system to different types of operations and the universality and high degree of automation permit its use in flexible manufacturing systems. These advantages make it possible to develop assemblies and parts for a broad product mix at an essentially new level, with higher degree of technological effectiveness and reliability in reducing the number of production operations and in reducing the time of manufacture of new machines and mechanisms in small- and medium-series runs.

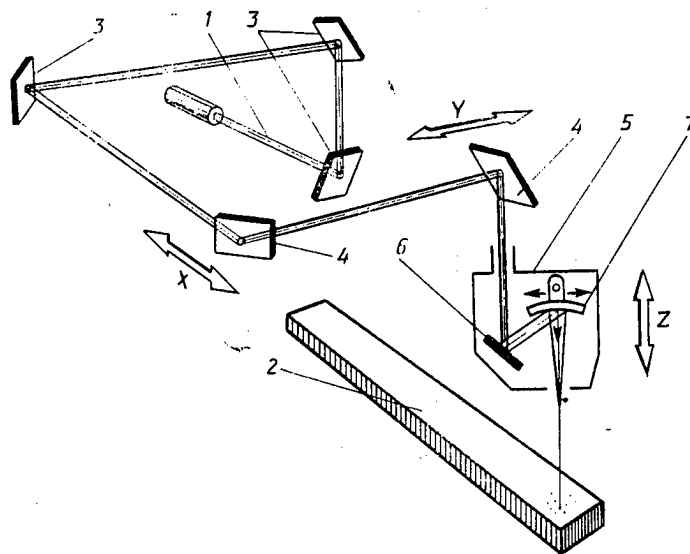


Figure 7. Laser Machining Layout

The equipment of the system--a laser machining module--consists of a high-power production CO<sub>2</sub> laser, high-precision positioning system, transport system that supports continuous machining of parts measuring up to 2,500 x 1,000 x 1,000 mm and a unified control system.

The laser path (Figure 7) delivers a laser beam from laser emission source 1 to the part to be machined 2. Refractive mirrors 3 are fixed and mirrors 4 are moved along the X and Y axes, respectively. The optical head 5 is moved along the Z axis. The beam impinges on fixed mirror 6, then on focusing mirror 7, which can be oscillated at high frequency if necessary, creating a scanning effect. The layout permits rapid readjustment from one type of laser machining to another.

The first Soviet models of industrial tooling and equipment for manufacture of castings by the vacuum film molding method were presented by VPTIlitprom [All-Union Design and Production Institute of the Foundry Industry]. Vacuum film molding is a progressive and promising continuous method of producing castings in sand molds. It occupies an intermediate position in the quality of the cast surface and size and weight accuracy between castings produced by chill casting and castings produced by smelted models.

The use of this method improves the working conditions in the foundry. The technology of vacuum film molding is universal and can be used to manufacture cast blanks of different sizes from ferrous and nonferrous alloys.

The industrial tooling--molds and makeup plates--are distinguished from the competition by lower weight and labor intensiveness of manufacture and by high operating reliability.

The dimensions of the mold, in mm, are 500 x 350 x 100, 500 x 400 x 150, 740 x 640 x 150, 1,000 x 800 x 150 and 1,200 x 800 x 300.

The saving due to introduction of the technology, equipment and tooling comprises approximately 20 rubles per ton of finished iron castings.

The Institute of Automation and Electrometry, jointly with the SKB [Special Design Office] of Scientific Instrument Building, SO AN SSSR [Siberian Department, USSR Academy of Sciences], has developed an interference linear displacement transducer, introduced at the Scientific Production Association Optika (Moscow) and at the Central Institute of Computer Hardware (Sofia, Peoples Republic of Bulgaria). The transducer is designed to convert linear displacements to a pulsed electric signal, containing information about the extent, rate and direction of displacements, position and contour control of the movements of coordinate tables of scientific experiment installations and of lithographic equipment and also of the working members of metal cutting machines and measuring machines.

The transducer can be used in the counting and control systems of measuring machines and metalcutting machines, for active correction of kinematic and geometric errors of NC machine tools, for conversion of physical values expressed by length (linear displacements, angular rotations, speed, acceleration, vibration, pressure, temperature expansion of materials, level of liquid, deviation from linearity, roundness, cylindricity and so on) to a digital code.

The distinguishing features of the transducer are the use of phase modulation that creates a photoelectric AC signal at the output of the interferometer and also the use of a single-frequency laser, stabilized by the Lamb dip and having high reproducibility of wavelength.

The transducers are made in the form of a set of basic modules: a laser head, automatic laser emission frequency adjustment module, interferometer, measuring reflector, receivers and an adapter. The additional modules, not contained in the basic set, provide beam-splitting for transducing two-dimensional displacements, the ability to work with specular reflecting objects, measurement of angular revolutions and so on.

The working principle of the transducer consists of comparison of the displacement of an object to be checked to a natural constant--laser emission wavelength. The comparison is made by using a two-beam interferometer, the measuring arm reflector of which is attached to the object. A frequency-stabilized helium-neon laser is used as the emission source in the interferometer. The difference of the laser path in the interferometer is varied upon movement of the object and variations of the luminous flux from the maximum to minimum value is observed at its output. Interference signals are converted to sinusoidal electric signals by two photodetector receiver modules. The signals are further converted to a pulsed sequence, containing measuring information about the extent and direction of displacement, in a normalizing converter. The pulsed sequence includes a direction of motion signal and counting pulses, shaped upon displacement of the object every  $\lambda/8 = 0.08 \mu\text{m}$  ( $\lambda$  is the wavelength of the laser, known with relative error of  $5 \cdot 10^{-8}$ ). The wavelength conversion procedure requires passage through the reflector of the interferometer for the distance to be checked.

Phase modulation is used in the interferometer to eliminate the effect of the interference background and to improve the operating reliability of the transducer. Special attention was devoted during the development of the transducer to increasing the service life of the laser and also to increasing its vibration resistance.

#### Specifications of Transducer

Transducible displacements, m	0-3
	(possibility of increase to 30)
Discreteness of information on displacement, $\mu\text{m}$	0.08
Rate of displacements, m/min	0-18

[Specifications of Transducer continued.]

Transducing error, $\mu\text{m}/\text{m}$ , not more than	0.5
Number of coordinates to be checked simultaneously (when using one laser)	2
Ready time, min, not more than	3
Mean cycles between failures, hr, not less than	5,000
Service life, years, not less than	3
Overall dimensions of modules, mm:	
laser head	110 x 310 x 90
automatic frequency adjusting module	440 x 570 x 12
interferometer	55 x 70 x 50
reflector	75 x 65 x 67
receiver	200 x 80 x 40
adapter	160 x 160 x 30

A flexible automated section for integrated machining permits lathe and drill-mill machining of a broad product mix of parts in the automatic mode. The total weight of the equipment is 35 t, the overall dimensions are 18 m long and 12 m wide, the operating mode is 2-3 shifts and the product mix of products to be machined is 3-100 units. The production equipment of the section is combined by a single transport system. An ASU [Automatic Control System] controls the operation of the section.

The Rotor-1 transport robot is designed for transport, transloading and positioning of standardized containers with products in machining shops, included in flexible automated plants.

The load capacity of the robot is 200 kg, the accuracy of positioning in all directions is 5 mm, the accuracy of positioning a container on the table is 1 mm and the continuous operating time is 8 hr.

The programmable multipurpose automatic assembler, developed by the Production Association AvtoZIL, is designed for simultaneous assembly of different products with different manufacturing series. Each actuating mechanism of the automatic machine operates according to an individual program as a function of the type of product to be assembled at a specific position of the turntable of the automatic machine. Each position of the turntable is outfitted with a quick-change jig-type assembly fixture, installed in a pneumatic vortex vibration generator. The turntable is supplied with a six-program programmer.

The productivity of the automatic machine is 720 products/hr. The drive of the turntable and the jig-type assembly fixtures is pneumatic vortex type. The overall dimensions of the automatic machine are 1,800 x 1,500 x 1,250 mm and its weight is 350 kg.

The robotized production system (RTK) for assembly of industrial robots, developed by the Tula Polytechnical Institute, is used for automatic assembly of the solenoid-operated air distributors of industrial robots of the Universal mode.

The system includes two Ritm 01.01 industrial robots, two load holders and a pneumatic press assembler. All assembly operations are concentrated within a single robotized production system, supplied with an adaptive monitoring system and custom mechanical grippers. The drive of the loading unit is electrical.

The operating mode of the system is adjustable and automatic.

#### Specifications of Robotized Production System

Load capacity, kg	0.1 kg
Number of positions:	
load	8
assembly	1
Pressing force, N	up to 3,000
Time required to assemble a standard product, s, not more than	60
Air pressure, MPa	0.6
Overall dimensions, cm	120 x 100 x 175
Mass, kg	200

A flexible manufacturing module based on the STP-220PR NC lathe and the RM-104 industrial robot, is designed for automatic machining of parts of different structural materials and alloys in small-series broad product mix manufacturing.

The flexible manufacturing module includes a lathe, loading robot with movement in four coordinate axes and a computer-aided control system (numerical ASURTK [automated control system of the robotized production system]), executed according to the CAMAC standard. The industrial robot is installed on a rotary bracket.

#### Specifications of Flexible Manufacturing Module

Diameter of parts to be machined, mm	16-120
Rotational frequency of spindle, rpm	11.2-2,000
Number of tools in turret head, units	8-12
Time required to replace parts, s, not more than	15
Precision of robot positioning, mm	±0.3

COPYRIGHT: Izdatelstvo "Mashinostroyeniye",  
"Mekhanizatsiya i avtomatizatsiya proizvodstva", 1986

6521

CSO: 1861/27

## DYNAMICS OF START-UP OF ARTERIAL HEAT PIPE FROM FROZEN AND COOLED-DOWN STATES

Minsk INZHENERNO-FIZICHESKIY ZHURNAL in Russian Vol 51, No 5, Nov 86  
(manuscript received 25 Sep 85) pp 741-748

[Article by A.N. Abramenko, L.Ye. Kanonchik, and Yu.M. Prokhorov,  
Institute of Heat and Mass Transfer imeni A.V. Lykov, BSSR Academy of  
Sciences, Minsk]

[Abstract] The starting performance of heat pipes in the low-temperature range is analyzed on the basis of experimental data from a cylindrical heat pipe with arterial porosity structure. Its 0.165 m long evaporator segment had grooves cut and its 0.76 m long condenser segment contained steel meshes forming a wick, both inside a sheath made of an aluminum alloy. Ammonia, not corrosive to aluminum alloys, was used as working substance usable at temperatures from the 405.6 K critical point down to the 195.4 K triple point and storable for long periods at room temperature owing to its high saturation pressure. The test equipment included a vacuum chamber with necessary controls for operation in the adiabatic mode under boundary conditions of the third kind with radiative heat extraction into a nitrogen-cooled cryogenic stage. The longitudinal temperature distribution was measured with chromel-alumel thermocouples. In one experiment the heat pump was started with the ammonia frozen at 140 K (cryogenic stage at 103 K, coolant temperature in liquid heat exchanger 283 K or 313 K). In the second experiment the heat pipe was started with the ammonia in condensing and adiabatic zones cooled down to 185-193 K (cryogenic stage at 123 K, coolant temperature in liquid heat exchanger 253-294 K, temperature at evaporator exit 210 K). The coolant in each case was ethanol. The dynamics of start-up from each state, namely the surface temperature transient, and the effective heat transfer coefficient as well as the thermal flux as functions of time were determined on the basis of continuous temperature and power measurements. The results reveal a strong influence of the coolant and particularly its initial state on the start-up dynamics. Starting from the cooled-down state (ammonia near its triple point) is independent of the heat extraction rate. Starting from the frozen state (ammonia below its triple point) is normal, when the initial heat extraction rate is near zero. Figures 4; references 12: 9 Russian, 3 Western.

2415/9835  
CSO: 1861/116

DYNAMICS OF ICE FORMATION ON UNDERGROUND PIPELINES

Minsk INZHENERNO-FIZICHESKIY ZHURNAL in Russian Vol 51, No 5, Nov 86  
(manuscript received 29 Jul 85) pp 802-809

[Article by B.A. Krasovitskiy, All-Union Scientific Research, Planning and Surveying Institute of Water Pipelines, Moscow]

[Abstract] Heat transfer from water flowing through an underground pipeline to the surrounding medium is analyzed on the basis of heat balance during the transient period under conditions favoring ice formation on the inside pipe surface. The equations of heat flow through water, pipe wall, and soil are solved for the appropriate initial and boundary conditions. Their solution by the method of numerical integration has been programmed in FORTRAN-5. Typical results are shown for icing during laminar flow of pure water and for turbulent flow of water with a solid phase (density  $1400 \text{ kg/m}^3$ ) in suspension. Calculations in the latter case can be simplified, considering the rapid buildup of ice at the front edge of a pipe and the subsequent small variation of the ice thickness along that pipe with a large and slowly decreasing temperature gradient. Figures 2; references 11: 6 Russian, 5 Western.

2415/9835

CSO: 1861/105

OPTIMUM PARAMETERS OF PUMP-TURBINE AND THEIR RELATION TO HYDRODYNAMIC CHARACTERISTICS OF BLADE ROWS

Moscow ENERGOMASHINOSTROYENIYE in Russian No 10, Oct 86 pp 2-4

[Article by A.K. Malyshev, engineer, and I.M. Pylev, candidate of technical sciences]

[Abstract] Design optimization of a pump-turbine is considered, taking into account the hydrodynamic characteristics of blade rows designed for reversible flow. The analysis is based on the model of one-dimensional flow and establishes the dependence of the efficiency in each operating mode on the speed and on the flow rate. Optimum speed and optimum flow rate, corresponding to maximum efficiency, are determined without accounting for the interplay of losses dipping to a minimum and losses monotonically increasing with the speed. This simplifies the relations, inasmuch as it allows the angle corresponding to shockless inflow to be regarded as optimum hydrodynamic angles. The optimum angle of stator blades is moreover assumed to be the same for both operating modes and to yield the optimum flow characteristics for zero angular component of the absolute velocity at the suction surface. The results of calculations agree with experimental data on single-speed pump-turbine units. References 9; 8 Russian, 1 Western.

2415/9835  
CSO: 1861/105

## ESTIMATING STATE OF STRESS FOR DESIGN OF DISKS FOR MIXED-FLOW TURBOMACHINES

Moscow ENERGOMASHINOSTROYENIYE in Russian No 10, Oct 86 pp 6-9

[Article by B.I. Berman, candidate of technical sciences, and V.V. Litinetskiy, candidate of technical sciences]

[Abstract] Rotors of closed construction with meander profiles, consisting of stacks of disks with radial blades and eccentric trapezoidal windows, have been developed at the Leningrad Polytechnic Institute for maximizing both efficiency and economy of mixed-flow steam turbines at high angular velocities (above 400 m/s). The design was based on stress analysis by the finite elements method in the approximation of a uniform temperature field, necessarily requiring preliminary laboratory and computer experiments. Disks with and without center hole were considered, for the low-pressure cylinders of type-I turbines K-300 and K-800 or type-II turbines K-1000. Circumferential and radial stresses were calculated as functions of two governing dimensions, disk profile thickness and hub width, on the basis of 43 configurations with either a variously tapered conical surface throughout or with a sharp transition to a plane surface segment. The maximum stresses in the weakest sections were thus determined for disks made of 34CrNi3Mo steel with a 0.2%-set yield strength of 760 MPa, with a Young's modulus of 20.4 MPa and a Poisson's ratio of 0.32, rotating at a speed of 3000 rpm. The calculations had been programmed in PL/1 for a YeS computer. Figures 6; references 4: all Russian.

2415/9835

CSO: 1861/105

UDC 621.515.001.5:621.922.025.004.6

## PREDICTING ABRASIVE WEAR OF CENTRIFUGAL SMOKE-EXHAUST FANS AND GRINDING-MILL BLOWERS

Moscow ENERGOMASHINOSTROYENIYE in Russian No 10, Oct 86 pp 17-21

[Article by Yu.I. Abramov, candidate of technical sciences, and B.A. Balusov, engineer]

[Abstract] Operation of centrifugal fan and blowers exhausting air with suspended ash or dust is examined for abrasive wear of blades by solid particles. The problem is split into two parts, flow of an incompressible nonviscous fluid idealizing the gaseous phase, with retention of continuity, and contact effects upon collision of a nondestructable atomized solid phase with a wearable solid barrier. The first part of the problem is formulated according to the method of curving streamlines for the interaction zone and for the free zone, in a semistationary system of coordinates and with the

Bernoulli constant defined appropriately for each zone. It has been solved on a YeS-1045 computer by the method of successive approximations. The second part of the problem is formulated in a stationary system of coordinates for a polydisperse solid phase containing particles of a material as hard as or harder on the Brinell scale than the material of blades. It has been solved on a YeS-1045 computer by a semiempirical method, parameters of absolute motion having been replaced with parameters of relative motion and particles of random shapes having been replaced with spherical ones equivalent in mass. Calculations for a 6500-11-4N3L rotor on various conically tapered hubs and for either quartz sand as model abrasive or metal dust in the Yuzhuralnikel (Southern Ural Nickel) Plant as real abrasive have yielded the wear rate  $W$  according to the relation  $W = cv^2$  ( $v$ - absolute velocity of air stream,  $c$ - abrasion coefficient dependent on angle of attack). Into account were taken influencing factors such as particle size, spacing of blades, rotor diameter and speed rather than angular velocity. Calculations have been refined so as to also yield the generally nonuniform distribution of wear over the blade with and the blade length as well as over the perimeter of the spiral shroud. Figures 6; tables 4; references 10; 8 Russian, 2 Western.

2415/9835  
CSO: 1861/105

DEFOCUSING OF MIRROR SYSTEMS DURING UNIFORM TEMPERATURE VARIATION

Ashkhabad IZVESTIYA AKADEMII NAUK TURKMENSKOY SSR: SERIYA FIZIKO-TEKHNICHESKIKH, KHIMICHESKIKH I GEOLOGICHESKIKH NAUK in Russian No 5, Sep-Oct 86 (manuscript received 7 Dec 84) pp 29-33

[Article by M. A. Gurbanyazov, I. I. Malysheva, D. V. Rozhdestvenskiy, V. G. Fokin and Ye. L. Shiyanskaya, Scientific Production Association Solntic Turkme SSR Academy of Sciences]

[Text] The focusing properties of mirror systems (ZS) may deteriorate not only due to temperature deformations of the elements, caused by a nonuniform temperature field, but also during uniform temperature variation of the structure, if the elements of the system are made of different materials, which differ by linear expansion coefficients.

Uniform heating of the structure with small temperature gradients is typical for night operation of the antenna installation and during irradiation of it by scattered solar radiation on overcast days. If all the elements of the structure are made of the same material, uniform temperature variation causes a geometrically similar increase or decrease of the dimensions of the mirror system while retaining the shape and ratios of the dimensions of the system as a whole and does not reduce the antenna amplification factor. Similarity is disrupted upon temperature fluctuations in mirror systems whose elements are made of materials with different linear expansion coefficients, which is related to displacement of the elements with respect to the calculated positions and to variation of the ratios of the dimensions of the system.

Uniform temperature variation of the structure may significantly effect the accuracy of the mirror system even during installation, if its elements are assembled and adjusted at night under stable atmospheric conditions. Since these operations are prolonged and since the ambient air temperature may fluctuate over a wide range, variations of the controllable dimensions must be taken into account by introducing corrections as a function of the actual temperature.

The mirror system experiences even greater distortions during operation, since seasonal temperature fluctuations occur over a wider range, while the effect of

solar radiation by day causes a general additional increase of temperature of the structural elements and considerable nonuniformity of the temperature field of both individual elements and of the structure as a whole.

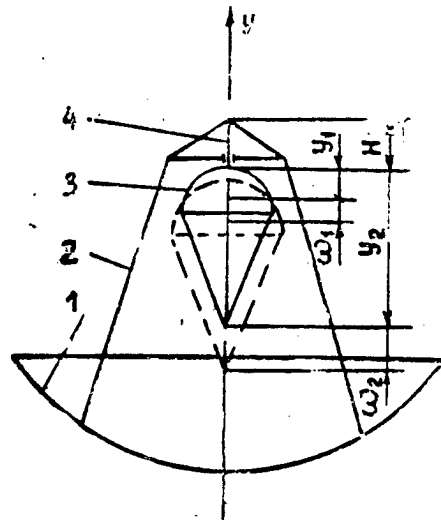


Figure 1. Structural Diagram of Mirror System: 1--main mirror; 2--support structure of counterreflector; 3--counterreflector; 4--guide counterreflector

The effect of a uniform temperature field on the geometric characteristics of the mirror system is considered on the example of a two-mirror system, made according to the Gregory layout, in which the main mirror 1 and the support structure of the counterreflector 2 are made of steel, while the counterreflector itself 3 and its guide 4 are made of aluminum alloy (Figure 1).

This combination of materials, the linear expansion coefficients of which differ by almost a factor of 2, is determined by the requirements placed on the counterreflector supports. On the one hand, they should have minimum cross-sectional area, since shadowing the aperture of the main mirror by the supports and counterreflector reduces the surface utilization factor and broadens the radiation pattern, and at the same time the supports should be sufficiently rigid and strong so that deformations and the corresponding displacements of the counterreflector do not exceed permissible limits when exposed to weight, wind and dynamic loads. These requirements are partially satisfied by selecting the optimal cross section of the counterreflector supports when using materials with high modulus of elasticity, and partially due to reduction of the weight loads, for which the counterreflector is fabricated from light structural materials.

Variation of the geometric characteristics can be fully characterized in two-mirror Cassegrain and Gregory systems with ideal surfaces by the relative displacements of the first and second foci of the counterreflector of the mirror system with respect to the focus of the main mirror  $w_1$  and the phase center of the irradiator  $w_2$ , respectively,

$$\omega_1 = \Delta\beta (y_1 + H) \Delta t, \quad \omega_2 = \Delta\beta (y_2 + H) \Delta t, \quad (1)$$

where  $\Delta\beta$  is the difference of the linear expansion coefficients of the counterreflector and main mirror materials,  $y_1$  and  $y_2$  are the distance of the counterreflector foci from the vertex,  $H$  is the dimensions of the guide from the point of attachment to the vertex of the counterreflector and  $\Delta t$  is the temperature deviation of the structural elements from the normal  $t_H = 20^\circ\text{C}$ .

The temperature of the structural elements in the absence of solar radiation can be assumed equal in the first approximation to the ambient air temperature, the range of which is determined from climatic data of the operating region of the antenna installation. A typical range of ambient air temperature variation is  $-40^\circ\text{C}$  to  $+50^\circ\text{C}$  for the USSR. The values of  $\Delta t$  fluctuate from  $-60^\circ\text{C}$  to  $+30^\circ\text{C}$ .

The relative displacements of the foci  $w_1$  and  $w_2$  along the axis of the system, calculated by formula (1), are equal to 0.0035 and 0.0082 m, respectively, for a mirror system with geometric dimensions  $y_1 = 1.4$  m,  $y_2 = 8$  m and  $H = 3.4$  m at  $\Delta\beta = 12 \cdot 10^{-6} \text{ K}^{-1}$  and  $\Delta t = -60^\circ\text{C}$ . If the surfaces of the mirror system are not precise, described by second-order equations, the resulting values of displacements (see Figure 1) only approximately characterize the variation of the focusing properties of this system.

Counterreflector and irradiator position correction systems are provided in modern large antenna installations to reduce the effect of weight deformations of the elements of the mirror system on radio engineering characteristics. Total compensation of the weight deformations is possible in mirror systems, designed on the basis of the homological deformation principle. A homological design of the main mirror in Cassegrain and Gregory mirror systems retains the parabolic shape at different elevations, that is, the initial paraboloid of rotation changes to a new paraboloid with different focal distance and direction of the focal axis. These variations of the parameters of the main mirror can be compensated for by automatic displacement of the counterreflector focus to a new point and by rotation of its axis. The fact that gravity is a constant factor makes it possible, by measuring the repeating error due to weight deformations during adjustment, to take into account using a control computer the variation of the parameters of the main mirror as a function of elevation.

Matching the deformations of the load-bearing structure of the main mirror and the support structure of the counterreflector as a function of the elevation due to displacements of the counterreflector along and perpendicular to the focal axis and its rotation in the elevation plane is provided in a number of designs, including the RT-70 [3]. With regard to variation of the ratios of the dimensions of the mirror system upon temperature fluctuations of the structural elements and thermal deformations of the structure, the adopted method of adjusting the counterreflector permits one to compensate for the displacement of only one of its foci. Displacement of at least two elements of the mirror

system is generally required for effective compensation of phase errors. Displacement of the counterreflector to combine its primary focus with the focus of the main mirror and displacement of the irradiator for combining the phase center with a secondary focus of the counterreflector in two-mirror Cassegrain and Gregory systems with ideal reflecting surfaces.

The geometric approach in problems of compensating for phase distortions, sufficiently effective for Cassegrain and Gregory mirror systems with ideal surfaces, is not applicable for mirror systems similar to the RT-70, in which the reflecting surfaces of the main mirror and of the counterreflector have the shape of a quasi-paraboloid and quasi-ellipsoid, respectively. The optimum displacements of the counterreflector and irradiator can be determined only by the phase compensation method [1], applicable to any surfaces matched by pairs. The criterion for estimating the operating characteristics of mirror systems is the reduction of the normalized amplification factor, dependent on the overlap of the optical path of the incident and reflected beams in the mirror system. In the case of axisymmetrical phase distortions, caused by displacements of the points of the reflecting surface of the counterreflector, the overlap of the optical path is determined as the projection of the displacement vectors onto the direction of the beam in an undeformed mirror system (Figure 2)

$$\Delta m(\rho) = \dot{m}_t \Delta t + \dot{m}_b b + \dot{m}_a a, \quad (2)$$

where

$$\begin{aligned} \dot{m}_t &= -[\bar{r}(\sin\alpha + \sin\beta) + (\bar{H} + \bar{y})(\cos\alpha + \cos\beta)]\Delta\beta \cdot R; \\ \dot{m}_b &= -(\cos\alpha + \cos\beta); \quad \dot{m}_a = \cos\alpha; \quad \bar{r} = r/R; \quad \bar{y} = y/R; \quad \bar{H} = H/R; \end{aligned}$$

$r = r(\rho)$ ,  $y = y(\rho)$  is the current radius and height of the counterreflector,  $\alpha = \alpha(\rho)$  is the angle between the incident and reflected beams on the main mirror,  $\beta = \beta(\rho)$  is the angle between the beam, impinging from the irradiator on the counterreflector, and the focal axis,  $\rho$  is the current normalized radius of the main mirror,  $b$  and  $a$  are the regulation displacements of the counterreflector and irradiator among the focal axis and  $R$  is the aperture radius of the counterreflector.

A reduction of the normalized amplification factor  $\Delta\kappa$  is determined by the formula [1]

$$\Delta\kappa = \frac{1}{2\pi} \int_0^s e^{-i2\pi \frac{\Delta m}{\lambda}} E(\rho) d\rho, \quad (3)$$

where  $\Delta m$  is the overlap of the optical path,  $E(\rho)$  is the amplitude distribution of the field in the aperture of the mirror system and  $\lambda$  is the wavelength of radio emission.

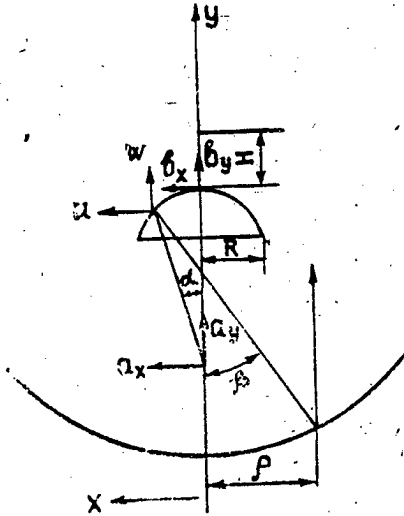


Figure 2. Path of Beams in Mirror System

Formula (3) can be reduced to the following form for calculation of  $\Delta\kappa$  [2]

$$\Delta\kappa = 1 - \kappa = 1 - \frac{\left[ \int_S E(\rho, \gamma) e^{j\psi(\rho, \gamma)} dS \right]^2}{\left[ \int_S E(\rho, \gamma) dS \right]^2}, \quad (4)$$

where  $\rho$  and  $\gamma$  are polar coordinates.

Phase distortion  $\psi(\rho, \gamma)$  and wave number  $K = 2\pi/\lambda$  are connected by the relation

$$\psi(\rho, \gamma) = K[\Delta m(\rho, \gamma) - \rho\theta K \cos\gamma],$$

where  $\theta$  is the angle between the optical axis of the undeformed mirror system and the axis, in the direction of which the antenna amplification factor is determined.

It is easy to show that expression (4) can be represented in the following form with respect to function (2)

$$\Delta\kappa = K^2(b, a, t) \cdot \begin{pmatrix} \delta_{bb} & \delta_{ba} & \delta_{bt} \\ \delta_{ab} & \delta_{aa} & \delta_{at} \\ \delta_{tb} & \delta_{ta} & \delta_{tt} \end{pmatrix} \begin{pmatrix} b \\ a \\ t \end{pmatrix}, \quad (5)$$

where

$$\delta_{ij} = \frac{\int_{-b,a,t} E m_i m_j \rho d\rho}{\int_{-b,a,t} E \rho d\rho} - \frac{\int_{-b,a,t} E m_i \rho d\rho}{\int_{-b,a,t} E \rho d\rho} \cdot \frac{\int_{-b,a,t} E m_j \rho d\rho}{\int_{-b,a,t} E \rho d\rho}$$

The optimum regulation displacements of the irradiator  $a^*$  and of the counter-reflector  $b^*$  to compensate for the phase distortions, caused by thermal deformations, are determined from the condition of optimality

$$\partial \Delta \chi / \partial a = 0, \quad \partial \Delta \chi / \partial b = 0.$$

The regulation displacements  $a^*$  and  $b^*$  and the values of  $\Delta \chi \cdot \lambda^2$ , which characterize the loss of amplification of the mirror system, are calculated for the mirror system of the RT-70 radio telescope, the structural diagram of which is similar to that presented in Figure 1. The calculation (table) was made at  $\Delta \rho = 12 \cdot 10^{-6} \text{ K}^{-1}$ ,  $\Delta t = -60 \text{ K}$ ,  $R = 3.5 \text{ m}$  and  $H = 3.4 \text{ m}$ .

Values of Regulation Displacements

(1) Параметры	(2) Тепловые деформации		
	(3) не компенсируются	компенсируются перемещением контррефлек- (4) тора	компенсируются перемещениями контррефлектора (5) и облучателя
$b^*$ , мм	—	—3.5	—2.1
$a^*$ , мм	—	—	7.3
$\Delta \chi \cdot \lambda^2$ , мм <sup>2</sup>	30	0.34	0.002

Key:

- |                         |  |
|-------------------------|--|
| 1. Parameters           | 4. Compensated by displacement of counterreflector                 |
| 2. Thermal deformations | 5. Compensated by displacements of counterreflector and irradiator |
| 3. Not compensated      |  |

Comparison of the results with experimental data, conducted on the RT-70 radio telescope [2], showed that a reduction of amplification is of the same order of magnitude in the absence of phase compensation of thermal deformations as residual losses of amplification after introduction of phase compensation of weight deformations.

#### Conclusions

1. The fraction of thermal deformations as an uncompensated component in the total loss of amplification increases as the working wavelength decreases; therefore, thermal deformations must be compensated when converting to millimeter

waves, by introducing feedback that reacts to ambient air temperature variation in the phase compensation system.

2. The phase distortions, caused by thermal deformations during uniform cooling of the mirror system, are essentially compensated for completely by the phase distribution, introduced by displacements of the counterreflector and irradiator.

#### BIBLIOGRAPHY

1. Kalachev, P. D., A. N. Kozlov, V. B. Tarasov and V. N. Titov, "Matching the Deformations of Mirror Systems of Fully Rotatable Radio Telescopes," NAUCHNYYE TRUDY FIAN, No 77, 1974.
2. Kozlov, A. N., F. L. Meshchanskiy, V. B. Tarasov, D. V. Rozhdestvenskiy, V. A. Grishmanovskiy, I. N. Knyazev, L. M. Fedoseyev, A. G. Gulyan and A. M. Aslanyan, "Full-Scale Investigations of the Operation on the Metal Structures of the 70-Mirror P-2500 Radio Telescope," "Nauchnyye trudy TsNIIproyektstalkonstruksiya" [Scientific Proceedings of the Central Scientific Research and Planning Institute of Assembled Steel Sections], Moscow, 1981.
3. Kozlov, A. N., V. B. Tarasov, V. N. Titov, V. A. Grishmanovskiy, G. N. Kolcheyev, P. D. Kalachev, B. S. Korobov and I. N. Knyazev, "The Mirror System of the RT-70 Radio Telescope," IZVESTIYA VUZOV. SERIYA RADIOFIZIKA, Vol 16, No 12, 1973.

COPYRIGHT: Izdatelstvo "Ylym".

"Izvestiya Akademii nauk Turkmenskoy SSR. Seriya fiziko-tekhnicheskikh, khimicheskikh i geologicheskikh nauk," 1986

6521

CSO: 1861/149

## TESTING AND MATERIALS

### CATALYTIC ACTIVITY OF NICKEL COATINGS, CHEMICALLY PRECIPITATED ONTO NONCONDUCTING MATERIALS

Kishinev IZVESTIYA AKADEMII NAUK MOLDAVSKOY SSR: SERIYA FIZIKO-TEKHNICHESKIKH I MATEMATICHESKIKH NAUK in Russian No 3, Sep-Dec 86 (manuscript received 11 Jul 84) pp 65-67

[Article by L. N. Andreyeva and Zh. I. Bobanova]

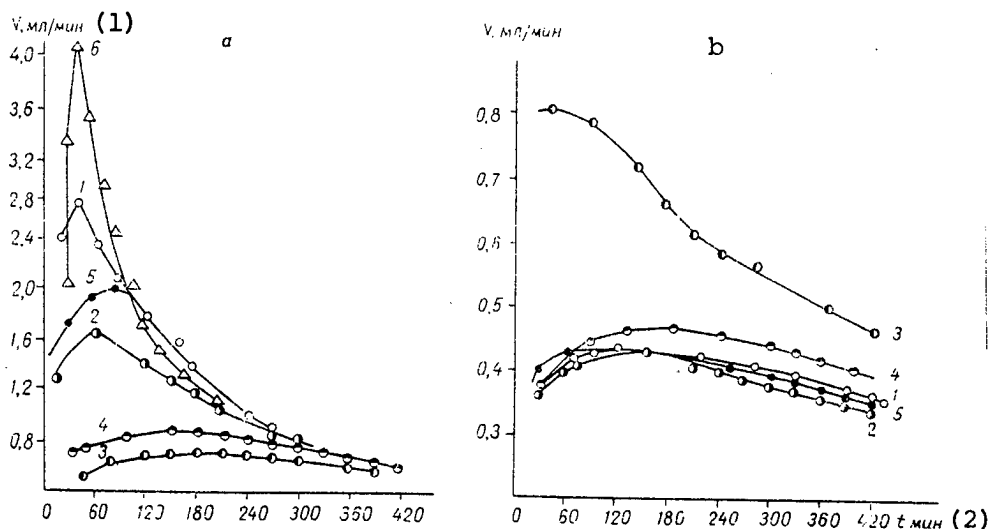
[Text] The catalytic activity of metals is determined by the physicochemical properties of their surface [1] The effect of the thickness and the heat treatment conditions of the nickel coatings on their catalytic activity in the  $H_2O_2$  decomposition reaction was investigated in this paper.

The nickel was precipitated chemically onto graphite fibers and silicon carbide filament crystals from a solution containing 29 g/liter nickel sulfate and 13 g/liter hydrazine sulfate at pH of the solution of 10 and temperature of 92°C. The amount of precipitated nickel coating varied from 3.5 to 25 mg/cm<sup>2</sup>. The coated specimens were heat treated in a hydrogen or helium flow for one hour at 300-450°C.

The kinetics of the heterogeneous-catalytic hydrogen peroxide decomposition process on nickel catalysts was studied at constant mixing rate in the 6N KOH solution. The rate of reaction was measured by the gasometric method in a device that makes it possible to conduct the entire experiment in a closed space. The KOH and  $H_2O_2$  solutions of specific volume were mixed in a reaction vessel, in which the specimen to be investigated was first suspended.

Investigations of the effect of the thickness of the coating on the catalytic activity of nickel, precipitated onto filament crystals and graphite fiber, showed that catalytic activity varies with thickness. The rate of decomposition of the peroxide decreases with an increase on the amount of nickel on the graphite fiber (thickness of the nickel precipitate) from 3.5 to 18 mg/cm<sup>2</sup>. A further increase of the amount of nickel to 22 mg/cm<sup>2</sup> causes an increase of catalytic activity. The high activity of nickel coatings can be related to the specific surface of the catalyst and to the activity of the unit surface area [2]. Earlier investigations [3] made it possible to find that nickel catalysts develop a large surface in a region of small degrees of filling. This increase

of the specific surface with small thickness of the precipitated coating probably determines the high rate of the catalytic decomposition reaction of hydrogen peroxide (see Figure, a).



Kinetic Curves of Decomposition of Hydrogen Peroxide on Nickel Coatings, Precipitated Onto Graphite Fiber (a), Where Amount of Precipitated Nickel,  $\text{mg}/\text{cm}^2$ , is: 1--3.5; 2--7.5; 3--18; 4--22 without heat treatment; 5--7.5, heat treated in hydrogen flow and 6--7.5, heat treated in helium flow, and SiC filament crystals (b), where amount of precipitated nickel,  $\text{mg}/\text{cm}^2$ , is: 1--7.5; 2--18 without heat treatment; 3--7.5; 4--18; 5--22, heat treated in helium flow

Key:

1. ml/min

2. min

The nature of the carrier affects the activity of the catalysts. Nickel coatings, precipitated onto graphite fiber, on which the rate of decomposition of hydrogen peroxide exceed by more than an order of magnitude the decomposition of hydrogen peroxide on nickel coatings, precipitated on filament crystals (see figure), showed the highest activity.

Heat treatment in a helium and hydrogen medium increases the catalytic activity of nickel catalysts and the rate of decomposition of hydrogen peroxide is dependent on the calcination temperature and on the environment of treating nickel coatings. The maximum activity was noted for heat treatment at  $400^\circ\text{C}$  in a helium atmosphere (see figure, a, curve 6). It was found that, when the thickness of heat-treated nickel coatings in a hydrogen atmosphere is increased, the catalytic activity decreases in the same sequence as for nickel catalysts, not subjected to heat treatment (see figure, b, curves 3-5).

The maximum catalytic activity (see figure, a) is more clearly manifested on nickel coatings, precipitated onto graphite fiber (curves 1 and 2) and especially after heat treatment of the nickel coatings in helium (curve 6) and hydrogen (curve 5) current.

The preliminary treatment conditions have a significant effect on the nature of interaction of the nickel and carrier. The nickel coatings are probably capable of forming surface complexes with the carrier as a result of heat treatment. One can assume that a Berthollet-type surface structure is formed during shaping [4]. These structures are valence-saturated and the atoms of the elements contained in them can be mutually activated. The activity of the surface metal structures (complexes) will be determined by the specifics of the physico-chemical properties of the active components and by the position of the d-elements in the periodic table.

#### BIBLIOGRAPHY

1. "Stroyeniye i svoystva adsorbentov i katalizatorov" [The Structure and Properties of Adsorbents and Catalysts], edited by B. G. Linson, Moscow, Izdatelstvo "Mir", 1973.
2. Ashmore, P., "Kataliz i ingibirovaniye reaktsiy" [Catalysis and Inhibition of Reactions], Moscow, Izdatelstvo "Mir", 1966.
3. Bobanova, Zh. I., and A. I. Yagubets, IZVESTIYA AKADEMII NAUK MOLDAVSKOY SSR. SERIYA FIZIKO-TEKHNICHESKIKH I MATEMATICHESKIKH NAUK, No 2, 1978.
4. Zubovich, I. N., "Kataliticheskiye reaktsii v zhidkoy faze" [Catalytic Reactions in the Liquid Phase], Alma-Ata, 1963.

COPYRIGHT: Izdatelstvo "Shtiintsa". "Izvestiya Akademii nauk Moldavskoy SSR. Seriya fiziko-tekhnicheskikh i matematicheskikh nauk", 1986

6521

CSO: 1861/142

## BRIEFS

CERMET GLUES--new DTK cermet glues can be used to easily glue the most diverse materials--for example, metals and glass, quartz and ruby. The glues harden at 40-60°C and the joints tolerate heating to 700°C. The use of the glues promises bright prospects in electronic equipment manufacture, since the electrodes no longer need to be welded-in at high temperatures in vacuum bulbs and there is no need to burn silver pastes into the ceramics. Many metals can be joined to nonmetals without usual consumption of silver, platinum and gold. The new adhesives were developed at the Institute of Chemistry, Urals Scientific Center, USSR Academy of Sciences.

[Text] [Moscow IZOBRETATEL I RATSIONALIZATOR in Russian 12, Dec 86 inside front cover] [COPYRIGHT: "Izobretatel i ratsionalizator", 1986] 6521

METAL FLAW DETECTION--a vibration device, developed at the Riga Polytechnical Institute, is capable of "shaking out" information about latent defects of the metal fuselage of aircraft, the glass fiber-reinforced plastic hull of ships and the polymer body of motor vehicles. The vibration exciters of the device, handling of which require no special training, create mechanical vibrations at the point of contact with the structure. The frequency of these vibrations, indicated on a lighted board, informs one of defects in the power elements of the structure.

[Text] [Moscow IZOBRETATEL I RATSIONALIZATOR in Russian 12, Dec 86 p 1]  
[COPYRIGHT: "Izobretatel i ratsionalizator", 1986] [6521]

CSO: 1861/146

- END -